



HAL
open science

Vibrational Characterization of the Various Forms of (Solvated or Unsolvated) Mobile Proton in the Solid State. Advantages, Limitations and Open Questions

Philippe Colomban

► **To cite this version:**

Philippe Colomban. Vibrational Characterization of the Various Forms of (Solvated or Unsolvated) Mobile Proton in the Solid State. Advantages, Limitations and Open Questions. *Solid State Ionics*, 2023, 393, 10.1016/j.ssi.2023.116187. hal-04009195

HAL Id: hal-04009195

<https://hal.science/hal-04009195>

Submitted on 1 Mar 2023

HAL is a multi-disciplinary open access archive for the deposit and dissemination of scientific research documents, whether they are published or not. The documents may come from teaching and research institutions in France or abroad, or from public or private research centers.

L'archive ouverte pluridisciplinaire **HAL**, est destinée au dépôt et à la diffusion de documents scientifiques de niveau recherche, publiés ou non, émanant des établissements d'enseignement et de recherche français ou étrangers, des laboratoires publics ou privés.

Copyright

Vibrational Characterization of the Various Forms of (Solvated or Unsolvated) Mobile Proton in the Solid State. Advantages, Limitations and Open Questions.

Philippe Colomban

Sorbonne Université, CNRS, MONARIS UMR8233, C49, 4 Place Jussieu, 75005 Paris, France

Philippe.colomban@sorbonne-universite.fr

ORCID : 0000-0001-6099-5423

Abstract.

A didactic review of (Raman, infrared and neutron) vibrational spectroscopy procedures to study mobile protonic species (H_2O , H_3O^+ , H_5O_2^+ , “ H^+ ”, NH_4^+ , etc.) in solid hydrates, crystals and ceramics is proposed on the basis of paper published since 1970s. Three materials are taken as representative examples: hydrated uranyl phosphate (HUP), oxonium, hydroxonium and ammonium beta- and beta“-aluminas and nominally anhydrous strontium/barium zirconate perovskite. Particular attention is given to the advantages of isotopic substitution and dilution measurements as a function of temperature and partial ion exchange. The vibrational signatures that we consider as being able to serve as references for the different kinds of proton species observed in the proton conductors are presented. We also discuss the signature of protonic species giving no vibrational signature - or whose Raman and infrared signatures are too weak to be clearly detected – that need to be better characterized and understood. The presence of a strong incoherent inelastic neutron scattering background appears characteristic of (mobile) proton conductors.

Keywords: Proton; oxonium; hydroxonium; infrared; Raman; neutron scattering; water pressure

1. Introduction

The proton, whose size is just halfway between that of the electron and the smallest of the "normal" ions, lithium, is a species apart. Ensberger in one of the first reviews devoted to the solid phase proton called it the "*nonconformist*" ion [1] and in a 1990s review paper [2] and book [3] on the determination of the proton and water composition of matter, I formulated Protonics as a new field of study, corresponding to Electronics for electrons and Ionics for ions. It is also noteworthy that Mendeleev had difficulty placing the element hydrogen in the periodic table and some scientists suggest placing H in the middle of the upper line, this (electron-free) element being able to exist as both a cation and an anion. [4,5] In the documents cited above as well as in reference[6], different procedures to detect the presence of protons and water in the solid phase have been discussed. The present review is far from exhaustive, its objective being only to give with three didactic examples the potential of vibrational analyses and in particular the combination of infrared and Raman or neutron spectroscopy to identify proton species, to characterize their nature, structure, bonding with neighboring moieties and host frameworks, and their dynamic and diffusive properties. In order to give a broader character to this review, attention will be also paid to solids hosting protons and hydrates of protons [7-17] similar to the selected materials discussed which present the diffusion or exchanges of protonic species. Indeed, as underlined in a previous review covering the study of proton conductors [11] since the (re)discovery of ionic superconductors in the 1970s, the work of the last decades has been focused on technological developments and studies to understand the interaction proton-host structure were dropped. Vibration spectroscopies which analyze the dynamics at different time scales of the local charge transfer, i.e. the first step of the conductivity process, have therefore been neglected from our point of view and this review aims to show their potential to non-specialists and to give a reference of the vibrational signatures of the different proton species leading to a proton mobility. We will discuss the implications that the spectroscopic findings have on the nature of the 'proton'-'host structure' chemical bond.

We will review the signature of the main proton species, from hydrates to the "isolated" proton in nominally anhydrous materials, then recall the characterization procedures of protonic species and details using vibrational spectroscopies, namely infrared, inelastic neutron scattering and Raman scattering, in particular for *in situ* and *operando* analyses. Indeed part of the practical procedures of analysis is rarely reported and their oral transmission lost when the practice of these procedures has not been maintained. We will underline how much the sampling preparation and the experimental procedure are decisive for the quality of the analysis.

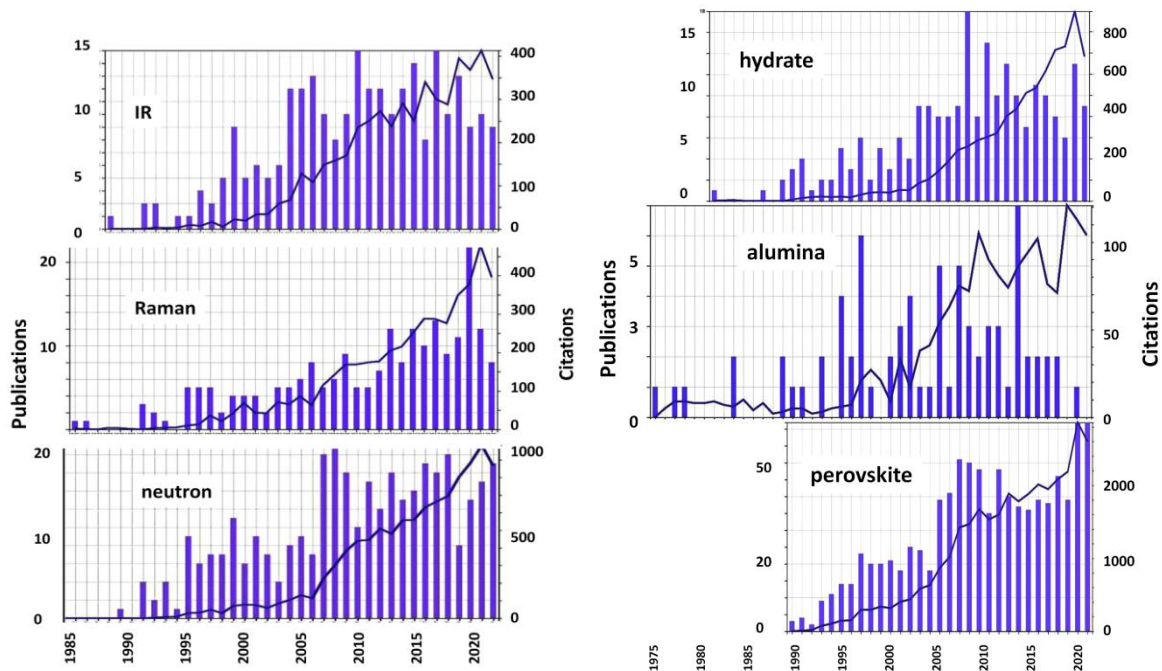


Figure 1. Comparison of the number of publications and citations per year for the keywords “IR”, “Raman” and “neutron” (left) and “hydrate”, “alumina” and “perovskite” (right) associated with “proton conductor” in the Web-of-Science® database (Clarivate Analytics).

Searching the Web-of-Science® database for the number of publications and citations concerning “proton conductors” indicates nearly 5,000 publications since the early 1990s with approximately 250 publications per year since 2000. The number of citations exceeds 150,000 with a rate of $\sim 15,000/\text{year}$ since 2010. As deductible in Figure 1, the proportion devoted to work using one or more vibrational spectroscopies concerns only less than 10% of citations and publications, this proportion having been greatly reduced over the years 2010. This is particularly clear for the infrared and Raman techniques. The identification of the content of the works from keywords is always imprecise and coarse but the overall evolutions give a global view. It is in particular without consulting each publication to differentiate the 'simple' characterizations from the in-depth spectroscopic studies and it is certain that the latter are in smaller numbers.

The examples we selected concern natural (mineral) and synthetic forms and they are chosen among those which seem to us to present the most relevant vibrational spectra from our point of view, among proton conductors, namely hydrated uranyl phosphate ($\text{H}_3\text{O UO}_2\text{PO}_4 \cdot 3\text{H}_2\text{O}$, conductivity $\sigma_{300\text{K}} \sim 5 \cdot 10^{-3} \text{ S/cm}$, activation energy: 0.35eV (250-370K range) [3,12]), beta (β) and beta” aluminas ($11 \text{ Al}_2\text{O}_3 \cdot 1.3 \text{ to } 1.6 [\text{H}_3\text{O}]_2\text{O}$, $\sigma_{300\text{K}} \sim 5 \cdot 10^{-6} \text{ S/cm}$, 0.2 eV (250-800K range) [3,13-15] and nominally anhydrous perovskites ($\text{SrZr}_{0.9}\text{M}_{0.1}\text{O}_{3-\epsilon}\text{H}_{0.005}$ (0.003 H_2O), $\sigma_{700\text{K}} \sim 10^{-2} \text{ S/cm}$, $\sim 0.3 \text{ eV}$ (700-900K, 20 bars H_2O) [16,17].

Figure 1 also compares the number of publications and citations concerning the keywords “hydrate”, “alumina” and “perovskite” associated with "proton conductor" to visualize the main work concerning the 3 selected compounds. We see the anteriority of work on beta aluminas and the strong development of those concerning perovskite since the years 2005.

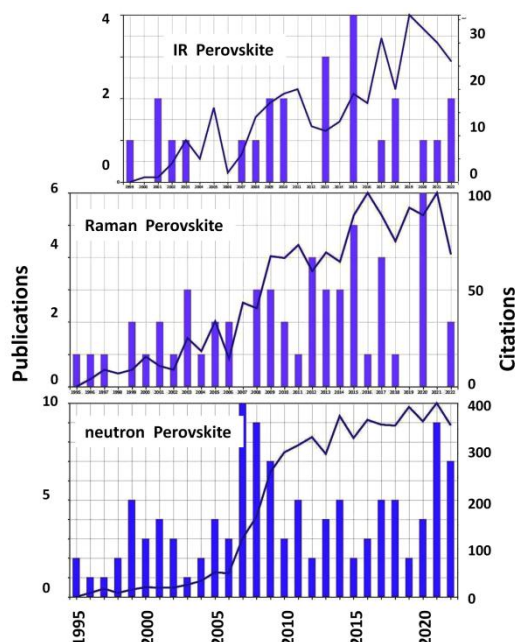


Figure 2. Comparison of the number of publications and citations per year for the keywords “IR”, “Raman”, “neutron” and “perovskite” associated with “ proton conductor” in the Web-of-Science® database (Clarivate Analytics).

Figure 2 visualizes the evolution of the number of spectroscopic works using infrared, Raman and neutron techniques concerning perovskite structures. The conclusions made generally indicated above are confirmed, scarcity of infrared studies and significant number of analyzes using neutrons, but a significant part concerns diffraction measurements, approximately 70%. The share of vibrational neutron spectroscopy is therefore comparable to that of Raman analysis.

Interest in materials exhibiting high mobility of the proton and / or water in the solid state has had a significant revival in recent years from the point of view of ecological concerns in order to develop devices for the production and storage of energy and CO₂ conversion based on the vector hydrogen. [2,11,18-22] We will not go into the biological material that is better associated with the liquid or gel state, and we will not discuss compounds where conducting protonic species are located at the surface of grains. [2,3] We will also show the necessity of the joint characterization of the same samples by vibrational spectroscopy and by crystallography. To our knowledge, no review has concerned the vibrational analysis of proton conductors since the chapter devoted to this subject in the reference book [3]. The variety of proton species that may be present in the materials does not

allow going in depth in the presentation of spectroscopic techniques and some references of basic works will be given.

2. The proton and protonic species in solid phase. Specificity and classifications

Geologists [7,23,24-26] and solid-state chemists [1-3,11-15,27,28] were the first to explore systematically 'mobile' protons in the 1970s, after the first oil crisis. In recent years there has been renewed interest in the presence of the hydrogen element in the rocks of the Earth's mantle (i.e. perovskites and associated compounds), the origin of the water constituting the seas remains strongly debated and the presence of protons being expected to strongly modify rock mechanics.[29-31] High conductivity of certain phases allowing the design of high performance electrochemical systems is also an origin of interest in fast proton conductors that can be used as an ion-exchanger, electrolyte or an electrode in devices in the hydrogen-based energy sector. [2,3,28,32-41] Thus, from the 1960s, the US and French programs respectively for the power supply of the Gemini space vehicle and submarine propulsion developed the first devices based on proton-conductor membranes, which were respectively polymers and ceramic. [3,11,32-41] Then the academic and industrial groups working on the hydrogen bond in the solid state, ion exchange compounds, electrochromic compounds, electrolytes and electrodes of batteries and fuel cells merged in a community looking for materials where the proton (solvated or not) is highly mobile [11] and attempted to better characterize and understand these species and their properties.

We note that the type of materials identified in these early studies (zirconia, perovskites and Nafion®) are practically the only ones that are used in industrial applications to date, most of the recent technological development deals with the improvement of electrode materials (decreasing of the quantity of – expensive - noble metal and then replacing noble metals with transition metals) and how to combine different materials in unit cells.

Indeed, the small size of the proton and its absence of electronic layers confers upon it a unique and very polarizing character [2,3] : the proton (also called protium) generally penetrates the sphere of coordination of other species and forms hydroxyl (OH^-), oxonium (also called hydronium) (H_3O^+), ammonium (NH_4^+), (di)hydrazinium (N_2H_5^+ , $\text{N}_2\text{H}_6^{2+}$), species which can be solvated by water molecules [2,3,42-46] to give H_5O_2^+ (hydroxonium), H_7O_3^+ ions, etc. [42] These species can be also evidenced in the gas state. [47] The extensiveness of the proton hydrate series is not mirrored in the analogous nitrogen containing family. It can be noted that the first *ab initio* calculation studies in the 1980s have concerned these proton hydrates. [48-50]

The high polarizing character of the proton gives a unique character to the X-H... Y bond [3,51] and to its vibrational signature: the distance, asymmetry and strength of the X – H... Y bond varies according to the respective acceptor (X) and donor (Y): in the H_5O_2^+ ion the O-H-O distance can be symmetrical and minimal at 0.24 nm³; the minimal distance from which the proton is considered to be free from hydrogen bonding is 0.295 nm.[2,3,51,52] As a result, the bond energy is variable: from around 40 kcal/mole for the strong symmetrical hydrogen bond in the H_5O_2^+ ion to less than 1 Kcal/mole for the weak bond. This has a direct importance on the dynamic behavior and its variation with temperature. At room temperature kT is equivalent to $\sim 200 \text{ cm}^{-1}$ or 0.6 kcal/mol. It follows that due to the weakness of the hydrogen bonds the proton species are in a dynamic equilibrium [53,54] from low temperatures, 150 or 200 K typically, which allows their rotational and/or translational ‘free’ movement (i.e. say rotational or translational diffusion), and associated properties (charge relaxation, conductivity, ion exchange, reactions) which are particularly attractive for certain applications. [2,11] A second effect of the high polarizing character is the easiness to detect species by infrared spectroscopy in combination with the large dipole induced by atomic vibration. Dipoles interact together which contributes to the broadening of the IR bands. This also facilitates the study of relaxation by conductivity analysis by complex impedance in the GHz range [11, 55,56].

The low mass of the proton also determines its mechanical behavior and consequently the shape/width of vibrational signature: its dynamics couples with most of the other modes of vibration which can lead to a strong broadening and a great complexity of the band shape according the complexity of H-dynamic behavior. In addition, the very polarizing character also induces strong electrical couplings: the $\nu\text{O-H}$ band broadens and the center of gravity shifts from $\sim 3650 \text{ cm}^{-1}$ (O-H vibrator free of an H-bond to $\sim 1000 \text{ cm}^{-1}$ or less with the strengthening of the H-bond (the strongest (and symmetrical) bond is observed in the H_5O_2^+ ion). [2,3,51] In the latter case, the specific shape of the O-H band is characterized with 3 maxima usually near 3200-3400, 2700-2900 and 2300-2600 cm^{-1} respectively, called A-, B- and C-bands which were first identified by Hadzi et al. [57,58] The origin of the A, B, and C bands has been discussed extensively. The main accepted explanation of band-shaping mechanism of the νOH pattern is the strong non-linear coupling of rapid νOH and slow O..H-O band with other modes. [58] The A-B-C feature is characteristic for a strong bond, as observed in many hydrogen phosphates, arsenates and selenates, organophosphoric and carboxylic acids, and in some silicates, etc. [59-62] Relationships have been established between the center of gravity of the νOH ‘band’ and the O..H-O distance.[51,52] At low temperature (namely below 50-100K), quantum processes make interactions and especially proton transfer more complex (intricate entanglement as observed for electron) [63-65] but this behavior will not considered in this review.

Another important characteristic to be considered for proton-containing compounds is the small gap between the temperature of solidification (273 K) and the boiling point of water (373 K at normal atmospheric pressure). As a result, the partial pressure of water vapor varies very strongly and is unfortunately rarely (and with difficulty) controlled. [2,3,66-68] It follows that the surface of a compound containing a proton species is rarely in equilibrium and therefore a great chemical gradient in water / proton content will be present from the surface to the core (bulk) of matter. This has a huge effect on the crystallinity (and the defects gradient from the surface) and the proton conductivity of many phases, especially when proton diffusion takes place at a particle surface.[2] In this transitional zone ("the skin") the entire phase diagram "anhydrous compound-water" will be found, i.e. all the different phases existing in the diagram are modulated by the kinetic conditions of growth. This compositional gradient is deleterious – and ignored - for many characterizations, for instance X-ray/neutron diffraction when powder is used but also vibrational analysis by ATR-FTIR due to the difficulty to avoid partial dehydration (and non-stoichiometry, phase transitions, disorder, etc.) of the sample skin, or adsorption of extra water molecules at the grain surface. The use of large single crystals limits (kinetically) the gradient and the number of surface species. The size of the object (and of grain, the grain boundary being a way to reaction) is then an important factor for many properties [67,69]: the number of atoms at, or near, the surface becomes the majority for nanometric particles and therefore all of the material is then determined by the (local) partial pressure of water (depending of the curvature of the surface), for which the conditions determine the analytical procedures. In polycrystalline ceramics, grain boundary also is very important.

The hydrogen bond and the structure and chemical activity of water vary greatly with temperature and pressure and this is used, for example, in the choice of the working pressure and temperature of electrical energy production devices (e. g. pressurized water in a nuclear reactor): the non-polar nature of supercritical water modifies strongly its corrosion behavior,[68] and hence the corrosive action of water is maximal between 600 and 700 K.

Several criteria are possible to classify compounds containing water / protons. The first criterion concerns the chemical composition: the water and proton content. A distinction is thus made between hydrates and nominally anhydrous compounds for which the proton content is small or in which protonic species can be considered as defects linked to non-stoichiometry, in a way similar to doping (as for electron, hole or vacancy). A second criterion of classification is the dimensionality of the structure, fibrous, layered or 3D, this anisotropy determining certain properties such as the diffusion and conduction of the compound in the single- or poly-crystalline state and the role of grain boundary. Anisotropy also determines the vibrational signature that can be recorded. The control of the partial pressure of water is all the more essential (but very difficult) as the dimensionality and the

size of the particles is small. It is thus possible to classify the compounds according to their sensitivity to the partial pressure of water. [2,3,6,11] Electrical conductivity, more particularly its intrinsic properties, activation energy (E_a) and the pre-factor σ_0 [2,3] are other most used and relevant criteria, but these criteria are determined by those first mentioned.

3. Procedures of characterization

We will first briefly recall the alternative procedures to vibrational spectroscopy that allows us to establish the presence of water and/or a proton. It is essential to measure the content of proton species and in particular to differentiate the contributions of the species adsorbed on the surface of the samples from those of the species in the bulk. Then we will detail the vibrational methods, in particular those using isotopic substitutions, $^1\text{H}/^2\text{D}/^3\text{T}$ (and $^{16}\text{O}/^{18}\text{O}$). Indeed, mass variation alters the wavenumbers of vibrational modes via reduced mass or moment of inertia and makes for a more reliable band assignment. [42,51,54]

2.1. Thermal mass loss

Before any spectroscopic study is undertaken, a thermogravimetric analysis is required. Crushed crystals or ceramics should be preferred to minimize the error due to the contribution of surface species. The demonstration of a loss of mass during heating above ~ 400 K in a vacuum or in a dry atmosphere can be considered as a first indication of the presence of adsorbed water. [6] Mass loss between 700 and 800 K corresponds generally to the de-solvation of proton (H_2O or NH_3 loss) and mass loss above 900 to 1400 K to the departure of residual protons, strongly bound to the host framework. The indicated temperatures vary according to the upper structure and coupling with a mass spectrometer analyzing the evacuated gases makes it a requirement to prove without ambiguity the nature of the eliminated elements. Indeed (surface) (hydroxyl)carbonation of many compounds is easy and departure of CO_2 takes place above 1200 K. Hydroxycarbonates are easily solvated and lose water around 700 K. Hydrates can lose water as early as 300K with more or well defined transitions. For instance Keggin salts (e.g. $\text{H}_3\text{AW}_{12}\text{O}_{40} n\text{H}_2\text{O}$ with $n = 29, 21, 14, 6, 1$ and 0, $M = W$ (PWA: phosphorus tungstic acid) or $M = \text{Mo}$ (PMoA: phosphorus molybdic acid), $A = \text{P, Si, As, etc.}$) [70] also called POMs (polyoxometallate salts) are a good example with transitions of water loss and varying degrees of crystalline structure changes at $\sim 300, 310, 340, 480$ and 700 K. [43] Hexa- [43-46,53] and mono- [43,46] hydrates offer nice examples of H_5O_2^+ and H_3O^+ ions precisely analyzed by combining X-ray and neutron diffraction measurements at different temperatures. The change in value of n is a function of the bonding with the host network and hence depends both on the temperature and water pressure but very often the water and proton content remains

undetermined. [6] The water of hydration of the ions leaves below ~ 500 K at usual water pressure while the departure of the proton occurs generally above 700K. The departure of the last protons up to 1400 K highly depends on the type of structure. [6,67] The kinetics can be slow and the trapping of water molecules in the sample can give an apparent reversibility in the phenomenon of dehydration-rehydration if the heat treatment time is not long enough. The results are thus different depending on whether the sample is a single crystal, a dense or porous polycrystal or a powder if equilibrium times are too short. [6,67] The differentiation between the water molecules present on the surface or part of the structure is always subtle. Comparing the mass losses between the powder form and that of a dense polycrystalline sample (powder or sintered) or better still of a single crystal, [2,3,6,67] makes it possible to assess the relative proportions, but this is not always possible. The differences in bond strength of different types of "water", surface or bulk, in different forms (OH, H₂O, H₃O⁺ ...) allows the differentiation between thermogravimetric (TGA) and differential thermal/scanning (DTA/DSC) curves. [71] We will see later that vibrational analysis allows this differentiation with more confidence.

2.2. Infrared, Raman & neutron spectroscopy procedures

Infrared spectroscopy: The very polarizing nature of the proton induces a very strong dipole moment which means that IR spectroscopy is in many cases the most efficient method to detect and study protonic species, the vibrational modes involving the proton being intense and located in a different energy range from those of the other chemical species. However, the contribution of water adsorbed at the grain surface can dominate and obscure the signal of other protonic species. The very process of infrared spectroscopy originating from dipolar interactions, the infrared bands are as wide as the Coulombic couplings are possible, which is the case with X-H modes. For a long time two procedures were in the majority, the transmission analysis of a "IR transparent" pellet in which a small powder fraction (a few mg) of sample was dispersed by mechanical mixing with a mortar in a powder of a material that not absorb infrared radiation. The pellet is densified under pressure by cold sintering which requires the application of pressure for several minutes and traces of humidity at the grain surface promote the pressure sintering up to transparency. To avoid an increasing background due to the scattering of IR radiation by the grains or the pores, the grains must be almost submicron and the densification very high: the pellet should be thin (thickness < 500 μm) and look translucent. KBr and NaCl are commonly used on instruments that do not access wavenumbers below ~ 400 cm^{-1} . [72] For measuring lower energy modes, CsI is preferred up to ~ 30 cm^{-1} and polyethylene is the required up to ~ 10 cm^{-1} . It is important that the KBr/NaCl or CsI powder has been dried at ~ 400 K to eliminate the contribution of excess water absorbed on KBr/NaCl/CsI grains (ca. 3200 cm^{-1} band) but too much

drying makes densification under pressure difficult and slow and the dried matrix will dry also the sample! Actually, more important and annoying, these compounds are not inert, and react/dissolve with water, and exchange their cations with H^+ or H_3O^+ (these phenomena are critical for compounds where the proton and water molecules are mobile). TlBr-TlI (KRS5[®]) is less reactive and is sometimes preferable. Therefore two methods should be preferred: the analyze of single crystal by transmission or reflexion and the mull method involving the dispersion in an inert liquid such as paraffin oil (commonly called Nujol[®]) and its fluorinated counterpart (Fluorolube[®]): the emulsion is prepared in agate mortar (in a glove box under controlled atmosphere), then deposited as a film between two single crystalline wafers of CaF_2 , KRS5 or CsI in a cell where polymer seals allow the emulsion to be isolated from the atmosphere [72-74] and therefore to permit the handling of samples where the H is partially or totally replaced by 2D or even 3T and ^{16}O by ^{17}O (for NMR analysis) [75-77] or ^{18}O [73] by using a glove box with controlled atmosphere. When the proton and/or water are mobile enough, it suffices depending on the case to place the compound to be exchanged near D_2O (exchange by vapor transfer) or in D_2O , if necessary in a sealed tube brought to a temperature sufficient to obtain a partial or almost total isotopic exchange. [78] This type of cell can be cooled to liquid helium (\sim below 50 K) [79] and be heated to a few hundred K (\sim 400-500K). [79,80] The cell is loaded if necessary in a glove box where the partial pressure of water is minimized by pure P_2O_5 powder or controlled by specific mixtures, molecular sieves or a gas controlled after pumping under vacuum. To avoid any risk of pollution, the faces of CaF_2 (in combination with Fluorolube[®]) or of KRS5[®] in combination with Nujol[®] or Fluorolube[®] should be preferred: KRS5[®] is transparent up to $\sim 100\text{ cm}^{-1}$. The very high transparency of CaF_2 allows very beautiful spectra above 1400 cm^{-1} but the easy cleavage of the crystal requires a certain skill in the tightening of the specimen cell.

Another technique is to use a very thin polished ceramic wafer or a single crystal obtained by cleavage : thickness less than 500 μm , or even up to 50 to 20 μm , so as not to saturate the modes of the host lattice is required. This technique has been used with profit for the study of a cleaved single crystal of beta alumina [42,81,82] (the very anisotropic structure of alumina makes the cleavage relatively easily) and polished perovskite ceramics [66,83]. A beam condenser or an IR microscope equipped with Cassegrain objectives is generally required. [42,81-84] In rare cases when the object is 'naturally' thin (such as a polymer fiber or film) direct measurements can be made [78,84]. Access to very low wavenumbers requires suitable instruments. Measurement is easy with thin ceramics or crystals but for powders the use of polyethylene windows or matrix (pellets) is required. Their handling is delicate, in particular the preparation of the pellet. This domain, which is now called THz, can be measured now with devices other than infrared spectrometers. [85] Polished crystals and ceramics make possible reflectivity measurements. Kramers-Kronig and Kubelka-Munk

calculation methods restore the Transmission/Absorption spectrum. Issues related to the modification of very wide bands in the KK/KM transformations will not be discussed.

The desire to reduce the preparation work has led in recent decades to the development of methods such as DRIFT (Diffuse Reflectance Infrared Fourier Transform Spectroscopy) and ATR-FTIR (Attenuated Total Reflectance- Fourier Transform Infrared). Methods are very simple: deposition of a little powder on the instrument. The spectrum is obtained by the evanescent wave from a diamond or germanium crystal in gentle contact with a powder (or a polished sample). [72] Measurements can be made from ~20K to 700 or 800K with specifically designed cryostats and heating cells. These methods are to be avoided in the study of protonated compounds because the probed thickness is variable (from ~2 to 10 μm in-depth, typically) according to the wavenumber and the optical property of the sample. Consequently, the measurement favors the surface, which is therefore a strongly disturbed region, [61] especially because the partial water pressure is rarely controlled and in equilibrium with the sample.

Neutron spectroscopy: The exceptional incoherent cross-sectional value difference between the ^1H isotope (80.26 barns) and the other elements, typically of the order of 1 barn or less, except for rare elements like ^2D (2.05 barns), means that an incoherent (or inelastic) neutron spectrum (INS) is in the first order of the modes involving the displacement of hydrogen atom. [2,3,6,86-102] In addition, the modeling of the spectra is reliable. Complete information can be found on reference textbook [86-89] The resolution of many instruments was mediocre in comparison with that of IR spectroscopy, and becomes worse, when the wavenumber becomes large ; moreover measurements are only possible below 200K with most of instruments. To date new instruments however shows combination of high resolution and large spectral window. As sketched in **Figure 3** neutron analysis using both instruments dedicated to diffraction (3-axis spectrometers) and specifically to dynamics (times-of-flight and back-scattering spectrometers for quasi-elastic and inelastic neutron scattering measurements) provides information on the structure and dynamics of H-based species characteristics and properties. The so-called $P(\omega)$ spectrum corresponds to the projection (density of state) of the spectra measured in the horizontal plane at different values of the wave vector. The background of the diffraction pattern (i.e. coherent neutron scattering measured as a function of wave vector for proton conductor) consists of the contribution to the incoherent scattering, i.e. the H-content. The quasi-elastic neutron scattering (QENS) signal allows a precise measurement of the H content and its evolution as a function of temperature. [2,3,6,11] It can be used as thermogravimetry to study the H-content as a function of temperature. [67,91,92] Very interesting information related to the proton mobility is extracted from the evolution of the quasi-elastic scattering as a function of the temperature and the comparison with the conductivity σ (Figure 3c, actually $\sigma \times T$ to visualize the

activation energy which corresponds to the slope of the line obtained). [3,90-93] Relaxation times and/or jump distance of the protonic species can be extracted from the QENS spectra measured at different wavevectors (Q) [93-102] and from impedance complex measurements in the GHz range [55,56]. Some instruments give a large part of the space explored in wavevector and wavenumber, it is useful to use all the information characterizing the compound: structure, H-content and dynamics. The conditions of access to the instruments and need for a large quantity of material (a few grams) for compounds containing little hydrogen unfortunately strongly limits the use of these techniques. See a comprehensive review of studies up to ~2010 in reference [67].

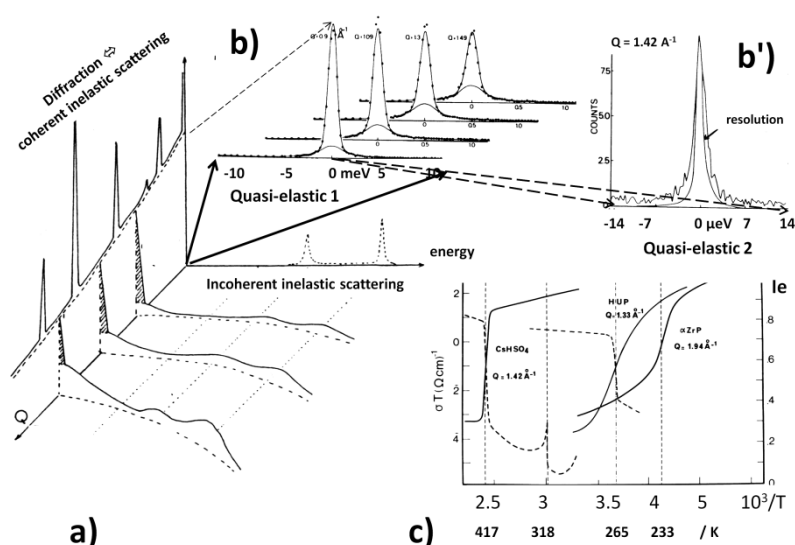


Figure 3. Schematic representation of coherent (diffraction) and incoherent (spectroscopy) neutron scattering adapted from [11] (a); detail for different energy windows of the quasi-elastic part of the spectrum measured at different wave vector (Q) (b,b', example of β alumina). In c) comparison of the evolution as a function of the inverse of the temperature (in K) of the intensity of the incoherent quasi-elastic peak with the measurement of the normalized conductivity (σT) for 3 proton conductors: CsHSO_4 , phosphate hydrated uranium (HUP) and hydrated zirconium phosphate (α ZrP); see references [11,91,92,49-105] for more details.

Raman Scattering: It is accepted that one of the interests of Raman analysis is the low vibrational contribution of water, which allows the study of species in the aqueous phase. [106] The intensities of the spectra of the proton/hydrate species will therefore be low and possibly very low. Luckily, the low mass of the proton generally means that the vibrational signature is in a spectral range where inorganic compounds do not contribute ($1500\text{-}4000\text{ cm}^{-1}$). Due to the low intensity of the Raman signature of water, those signals of proton species bearing charge (ionic species) are generally stronger and their spectrum can be measured. On the other hand, the light-matter interaction

process being different from the IR absorption, the Raman peaks will have reduced widths allowing better structural and dynamic differentiation. This is especially useful for the study of isotopically diluted ($H \sim 5\%$, $D \sim 95\%$) samples. [72,73,74,78] Since the measurement of narrow peaks is much less disturbed by the continuous background than for wide bands, this disadvantage is offset by the increased sensitivity of photonic detectors. An incomparable advantage is the possibility of carrying out the analysis without difficulty through an optically transparent medium such as a sealed tube (NMR or Lindeman tubes) or in autoclave cells brought to different temperatures for *in situ* or *operando* studies [107-109] Another advantage is that it is much easier to record the low energy Raman spectrum than an infrared, from 40 to 100 cm^{-1} easily (the threshold value depends from the exciting laser wavelength), up to $\sim 5 \text{ cm}^{-1}$ [107] with advanced instruments (with 'supernotch' filters). The analysis of a material or of a combination of materials in operation or in an equivalent environment (autoclave) requires being able to be generally do this through an optical window [109] and to differentiate the spectral signatures of the different constituents. Measurement efficiency at very low wavenumber is however limited by examination through optical windows. The variable parameters can be spatial (position), [108-115] strain/stress/pressure/temperature, [111-113], electric field, [114,115] the nature of the gas or liquid in contact, etc. The procedures are therefore variable. Depending on the variation of the external parameters, the effect on the spectral signatures is also very variable: chemical reactions and transformations, structural distortion and phase transition, stress distribution, disorder and non-stoichiometry, etc. Raman analysis is generally carried out by excitation of visible light, an optical window (sapphire, CaF_2 , Si, glass) or a glass wall is sufficient and this has been used for several decades. The packaging of the operating system must be transparent to radiation and the material accessible specifically (through focusing using long working distance objective) or by signal contrast. For instance, aluminum alloys are transparent for neutron inelastic incoherent scattering.

2.3. Ion exchange and H/D substitution

It is important to present the methods of isotopic dilution and controlled exchanges. Most ionic and proton conductors easily exchange their mobile species by exposure to a high concentration of another mobile species, in the liquid phase (molten salt or concentrated solution) [13-15,24,28,40,42,61,116] or even in the gaseous phase (gas, plasma) [81,117,118] or with more difficulty in the solid phase (electrochemical cell); an electric field is added to control the diffusion. Structural determinations from single crystals or more imprecisely from powders by Rietveld refinement make it possible to know the sites preferentially occupied by the ions and a partial substitution makes it possible to 'isolate' a proton species in a defined site. [2,42] The X-ray and (coherent) neutron cross-section of protons (and even of deuterons although higher than that of

protons) being weak, the accuracy of proton location is poor, especially when the data collection is not made at (very) low temperatures. [67] For example before the 2000s the structures were made almost exclusively on single crystals (for example concerning beta alumina) [13,24,119], and after 2000 the Rietveld refining on powders becomes the common rule [67,120-131] for reasons of convenience: difficulty of having single crystals, length of collection times of diffracted intensities with a 4-circle diffractometer, whereas a powder spectrum is obtained quickly with a synchrotron. Hydration control is rarely done and at best more or less well sintered pellets are used.

The combination of vibrational spectroscopy and the partial substitution of protonic species in single crystals with other ions makes it possible to 'simplify' the spectra by limiting the sites occupied by the proton species and thus to refine the attributions. The H/D substitution shifts the X-H modes of vibration by known factors (according to the square root of the mass ratios ($\sqrt{2} \sim 1.4$) for the simple stretching modes, according to the ratio of the moments of inertia for the rotational modes, etc.) [51], which allows for a reliable attribution. In addition, the isotopic dilution (H \sim 5, D \sim 95) by removing the mechanical couplings between X-H vibrators greatly reduces the width of the modes, in particular at low temperature, which makes it possible to differentiate the structural disorder from the disorder due to the temperature-dependent dynamics of the protons. [54,73,74]

3. Proton and proton hydrates in the solid state

3.1. From proton hydrates to H-bond free protons

The 'standard' forms of what can be formulated as water in a solid formula established from thermogravimetry and elemental analysis are the 'lone' proton, water molecule (H₂O), the oxonium ion (H₃O⁺), the hydroxyl ion (OH⁻), and more bigger and rarer species (H₅O₂⁺, H₇O₃⁺ or even H₉O₄⁺, H₁₃O₆⁺). All of these species can have a specific dynamical disorder, rotational or translational. The structure of the H₃O⁺ and H₅O₂⁺ ions was determined from X-ray and/or neutron diffraction measurements (Table 1), at a temperature sufficiently low to obtain reliable conclusions (i.e. 100K or less) for different phases [54,59,60,63,87-91] and/or from IR, Raman or neutron vibrational data, recorded at various temperatures. [66-75,92] Indeed both the precise structural determination (by structure refinement) and the recording of inelastic neutron and IR/Raman spectra require measurements at low temperature when the protons do not diffuse significantly. The measurement is therefore far removed from the temperature range where the material is 'interesting' for application. The proton, and even the deuteron, have a weak coherent section, either for X-ray and neutron scattering, which complicates their localization, all the more because of the strongly anharmonic character of their thermal agitation. Imaging the distribution of the residual

electronic/atom distribution by Fourier maps is required in order to evaluate the imprecision of the structure refinement and thus localization of the proton is difficult. This is why IR and Raman spectra that can be recorded over a wide temperature range are more informative than diffraction at a temperature where the compound exhibits (fast) ion conduction (i.e. a large distribution of mobile ions over the 1D, 2D or 3D conducting pathways).

The perturbations observed for the unit-cell (diffraction) and the fingerprint (vibrational spectrum) of framework hosting protonic species are often the best tool to follow the modifications generated by the protonic species and hence evaluate their behavior. Nevertheless it is necessary to correlate the low temperature diffraction data – and those performed at higher temperature - to the data obtained at the same temperature.

Figures 4 and 5 show representative infrared spectra, recorded on hydrated uranyl phosphate (Figure 4) and β alumina (Figure 5) of the most common protonic species: hydroxyl, oxonium and hydroxonium ions. Typical Raman spectra of oxonium and ammonium ions are given in Figure 6.

Although the combination of diffraction and vibrational spectroscopy allows a good knowledge to be obtained of oxonium, hydroxonium and ammonium ions, the structure of species larger than H_5O_2^+ is deduced from vibrational data. Some representative references are listed in Table I [41,42,43,47,58-61,65,66,91-102,120-131] and representative spectra in Figures 3 (hydrated uranyl phosphates) and 3 (beta aluminas). Information on other frameworks hosting H_3O^+ and H_5O_2^+ ions can be found in references [103-145].

The first accurate structural determinations of H_5O_2^+ and H_3O^+ ions were made on perchloric acid [139]). Also in this compound the first evidence of superionic conductivity of a proton was demonstrated and the diffusion coefficient of protons measured accurately by many techniques: ^3T and ^{18}O diffusion, NMR, conductivity and QENS [75-72,101,146].

Species	Compound	Diffraction	Spectroscopy	Refs
H_3O^+	Perchlorate,nitrate,etc.	XR,nD	IR,Raman,InS	60,75,101,137,139
	β/β'' alumina	XR,nD	IR,Raman,InS	13,24,81,82,119
	PWA	XR,nD	IR,Raman,InS	43,46,53
	HUP,HUAs	XR,nD	IR,Raman,InS	25,27,54,71,73,74,
	Jarosite/romboclase	XR	IR,Raman,InS	102,133,134,135
	NASICON	XR,nD		136,142
	PANI	-	IR,Raman,InS	144,145
H_5O_2^+	beta-alumina	-	IR,Raman,InS	24,81,82,119
	PWA	XR,nD	IR,Raman,InS	44,45,46
	PANI	-		144,145
	Perchlorate,nitrate,etc	XR	IR	133,138,140
H_7O_3^+	β/β'' alumina	-	IR,Raman,InS	82
NH_4^+	β/β'' alumina	XR	IR,Raman,InS	13
	HUP,HUAs	XR		25
O-H ⁻	β/β'' alumina		IR	81,146

"H ⁺ "	Perovskite (zirconate)		IR,Raman,InS	62,67,83,109,125,126,128
	Perovskite (cerate)	nD		67,121,123,127
	Perovskite (niobate)	XR,nD		122,124,129

Table 1. Representative compounds hosting proton hydrates analyzed by X-Ray (XR) or neutron diffraction (nD) and Infrared (IR), Raman and neutron inelastic (InS) spectroscopy.

3.1.1. HUP and KUP

We will first take hydrated uranyl phosphate (HUP) and arsenate (HUAs) as an example. These natural and synthetic compounds have a lamellar structure, quite comparable to that of clays, but the layer is made up of phosphate or arsenate ions bound to uranyl ion [23,25-27]. It was in the study of these compounds that J. Beintema in 1938 identified for the first time the proton as a 'wandering ion in the solid phase' [23]. With its remarkable conductivity and its ease of densification under pressure, this compound could have had numerous applications if it were not a uranium (and arsenic) salt. Many beautiful works have been done, such as the first all- solid display systems [147], the first all-solid supercapacitors, etc. [148,149].

Between these rigid uranyl phosphate/arsenate sheets (Figure 4), squares of 4 water molecules on two levels share a proton. The oxonium ion (HUP) can be replaced by K⁺ (KUP), Na⁺ (NaUP) and Li⁺ (LiUP) ions with small modifications of the spatial organization of the ion with respect to water molecules [23,25-27]. Similar features are found for arsenates. At room temperature, the ν O-H stretching spectral region exhibits a broad feature extending from ~ 2000 to 3800 cm^{-1} , even at 130 K, whether for HUP or the analogs KUP, NaUP and LiUP [54,73,74]. A broad mode of δ O-H deformation is observed around 1650 cm^{-1} , characteristic of water molecule to be compared with the 1750 cm^{-1} mode observed in HUP, characteristic of oxonium ion. After deuteration the bands are better structured (the doublet is clear) and we can distinguish the signature of ν O-H modes of water and oxonium [73,74]. Magnification of the upper wavenumber part of the spectrum ($2800\text{-}3800\text{ cm}^{-1}$ range) shows a spectacular narrowing of the band width with decreasing temperature. For instance, 4 modes are identified for HUP and at least 6 for KUP. The plot of the bandwidth (full width at half height) as a function of the temperature shows phase transitions corresponding to the onset of free rotation with respect to the hydrogen-bond when kT becomes higher than the potential well barrier.[54] The comparison of the spectra of the compound KUP containing only water molecule with HUP where K⁺ is replaced by H₃O⁺ highlights the contribution of the latter ions with their different hydrogen bonds, with neighboring water molecules and with the oxygen ions of the phosphate sheet. The main contribution of oxonium ion is around 2900 cm^{-1} (C-band) which will be also found in fully hydrated beta-alumina (Table 2). The presence of the K⁺ ion leads to the weakening of certain hydrogen bonds giving the very fine modes around 3450 and 3500 cm^{-1} : the

highest ν O-H modes in HUP are at $3380\text{--}3390\text{ cm}^{-1}$. Substitution of ^{16}O atoms by ^{18}O atoms starting with the synthesis from ^{18}O -labeled water gives complementary criteria for these and assists their assignment [72,74].

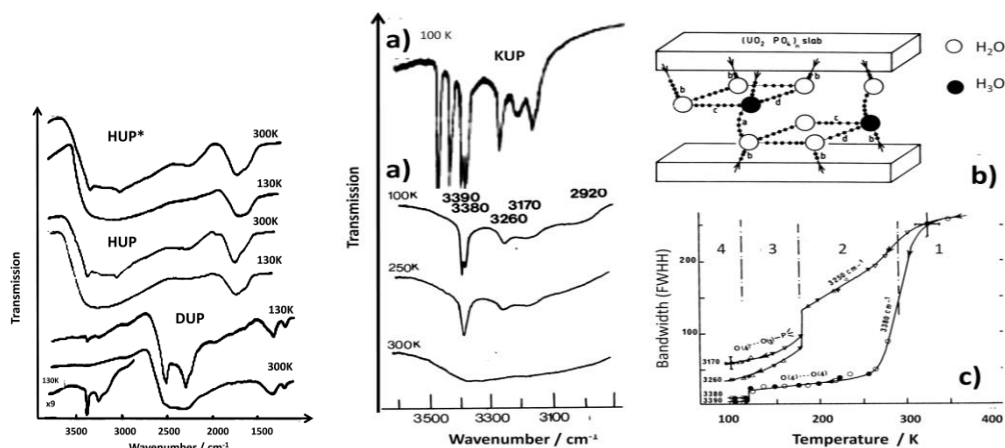


Figure 4. Comparison of isotopic diluted ($\text{H}/\text{D}\sim 0.1$) infrared spectra measured for KUP (a), at 100K and for HUP (a) at different temperature; b) schematic of the layer structure of HUP; c) evolution of the bandwidth (Full Width at Half Height) of the different O-H stretching modes as a function of temperature for HUP.

The monitoring of the temperature evolution of the width at half-height of the bands relating to each O-H vibrator of the isotopic dilution makes it possible to see the phase changes of the sub-network that constitutes the layer of acidic water. Each change corresponds to the transition to an orientation disorder with respect to the hydrogen bond and at the upper temperature to a translation (diffusion) disorder of the proton. This example shows the power of the infrared procedure coupled with isotopic dilution, a procedure rivaling the alternative methods of H-NMR (spin echo or MAS-NMR) and quasi-elastic neutron scattering, methods requiring much more expensive instruments.

Raman spectroscopy is also very efficient to study the $\text{UO}_2\text{P}(\text{As})\text{O}_4$ framework but the low intensity of ν O-H modes imposes long counting times and IR technique was preferred in the studies. [72-74]

3.1.2. beta and beta'' aluminas

Aluminates of sodium, lithium, potassium, etc. which are incorrectly called beta alumina because their composition $11\text{ Al}_2\text{O}_3 \cdot 1\text{ to }1.6\text{ M}_2\text{O}$ misled the people establishing the first $\text{Al}_2\text{O}_3\text{--Na}_2\text{O}$ phase diagram. These anisotropic compounds (Figure 5f) have a structure alternating compact layers of oxygen ions of spinel structure and an open layer (called the conducting layer) with a single oxygen ion forming the Al-O-Al bridge between up and down spinel blocks [13]. In this loose-packed layer several sites distributed on a honeycomb lattice are possible for the conductive ions (M^+ or M^{2+}). Periodic stacking faults give the phases beta''' and beta'''' [13-15,24,82,119]. The thermal stability of

the phases is very high, close to 2300 K. Sodium, potassium and lithium beta alumina are synthesized from the melt or by solid state reaction. [11,150]

Figure 5 compares the infrared spectra of H_3O^+ and H_5O_2^+ ions measured in transmission either on single crystalline beta (and beta ") alumina plates perpendicular to the c axis, i.e. the axis perpendicular to the planes where the conductive ions diffuse. The conducting plane is a mirror plane in the beta alumina structure. The spectrum recorded on powder, dispersed in fluorinated oil (fluorolube®) in between CsI windows is also given. [42] The ions were localized by structural refinement of the X-rays [13] in two different sites (usually called Beever-Ross (BR) and middle-oxygen (mO)) and their dynamics studied by quasi-elastic neutron scattering. [94] The mO and BR sites can be also filled with other ions (Ag^+ ions also occupied anti-BR site, at the corner of the conducting plane) to isolate the oxonium ions. Oxonium/hydroxonium and ammonium aluminates are prepared by ion exchange in acids or molten salts. [13,24,28,42] The spectrum of beta alumina powder of composition $11\text{Al}_2\text{O}_3 \cdot 1.3 \text{H}(\text{H}_2\text{O})_n$ with $n \sim 2$ (Figure 5b) shows a strong doublet at 3433 and 3395 cm^{-1} and a strong peak at 3508 cm^{-1} plus broad ABC bands at $\sim 3380, 2900$ and 2500 cm^{-1} due to residual H_5O_2^+ ions which become dominant when the compound is saturated with water (Figure 5c) [42,151]: in that case the oxygen ions of the proton species occupy all the sites to form an additional compact layer of oxygen ions in the conducting plane (perfectly in accord with compact oxygen atoms of the spinel blocks, Figure 5c), forming a water aluminate with spinel-like structure. Consequently thermal treatment of water aluminate single crystals is the only way to prepare single crystals of transition metal aluminas. [152]

The spectrum of the crystal where the H_3O^+ ions are in site BR (nearest oxygen ions of spinel blocks at more than 0.28 nm) shows only the peak at $\sim 3508 \text{ cm}^{-1}$. If the measurement is made on thin single crystal by transmission, only modes corresponding to the crystal set-up (Eu polarization) are visible: the second component of the doublet at 3508 and 3495 cm^{-1} observed for the powder spectrum is almost not visible. This band is absent for mixed $\text{Ag}^+\text{-H}_3\text{O}^+$ crystals and can be thus assigned oxonium ions located in mO sites [42]. These spectra can be considered as characteristic of an oxonium ion quasi-free from hydrogen bonding. The band is broadened in a mixed $\text{Ag-H}_3\text{O}^+$ beta" alumina crystal due to the high disorder of cation distribution along the different sites along the conducting honey-comb pathway in the conducting plane that induces a large distribution of hydrogen bonding [151]. Saturation with water (Figure 5a: powder; Figure 5c: single crystal) led to a spectrum dominated by the broadening of ABC bands characteristic of strong hydrogen bonds [2,3,57,58]. They were present at low intensity in the oxonium beta alumina spectrum due to the difficulty in the elimination of water from the conducting plane. These broad ABC bands are characteristic of the strongly H-bonded

and hydrated species, H_5O_2^+ and H_7O_3^+ (Table 2).[57,58] Note the great similarity with the spectrum recorded for HUP (Figure 4) in which these species are also present.

Table 2a: Main infrared OH stretching wavenumbers of H_3O^+ and H_2O species in KUP and HUP at 300 and 130/100 K for hydrogenated (H), deuterated (D) and isotopically diluted (isoH/D) compounds (after [73,74]); a comparison between the H-bond length deduced from the Novak' relationship [3,51] (a) with those from structural X-ray refinement (b) is given; isotopic wavenumber ratios are also given (S: strong; m: medium; sh: shoulder). Numbers 4 and 3 in brackets after the O indicates the type of oxygen atom in the unit-cell.

KUP(H) (cm^{-1})		KUP(D) (cm^{-1})		vH/vD		KUP(iso H/D) (cm^{-1})		d O...O ^a (pm) 100K	d O...O ^b (pm)300K	Assignment
300 K	100 K	300 K	130 K	300K	100/130K	300 K	100 K			
	3505 S	2500 sh	2600 sh	1.33	1.34		3480	0.285		
3460 S 3420 sh	3470 S 3445 sh	2560 S 2530 sh	2568 S 2550 S	1.35	1.35 1.35	3453	3450	0.283	2.83	v O[4]-H...O[4] (inter square)
3360 S	3405 S 3380 sh	2470 S	2518 S	1.36	1.35		3420 3410	2.81 2.80	2.80	v O[4]-H...O[4] (inter square)
3200 S	3290 m 3230 m 3150 S	2360 S	2460 S 2408 sh 2340 S	1.36	1.34 1.34 1.34	3300	3316 3270 3225	2.76 2.74 2.72	2.75	v O[4]-H...O[3] (O[3]: PO ₄)
1655 m	1675 sh 1660 S 1625 w	1220 m	1226 sh 1216 m	1.36	1.36 1.36		1460 1450 1416			$\delta \text{H}_2\text{O}$

HUP (H) (cm^{-1})		HUP(D) (cm^{-1})		vH/vD		HUP(iso H/D) (cm^{-1})		d O...O ^a (pm)130K	d O...O ^b (pm)300K	Assignment
300 K	130 K	300 K	130 K	300 K	130 K	300 K	130 K			
	3380 S	2540 sh			1.33		3390 3380	2.77 2.76	2.83	v O[4]-H...O[4] (inter square)
3350 S (A-band)	3320 sh 3220 S	2495 S	2505 S 2295 S	1.34	1.33 1.4	3350	3260 3170	2.71 2.69	2.81	v O[4]-H...O[3] (PO ₄)
	3060 S	2100 sh	2235 sh		1.37	2900	2920	2.63	2.56	v O[4]-H...O[4] (inter two square)
2600 sh (B-band)	2760 w	1900 sh	2000 m		1.38	Not detectable				
2300 sh (C-band)	2300 w					Not detectable				
1740 S	1780 S	1320 m	1330 m	1.32	1.34	1650 w				$\delta \text{H}_3\text{O}^+$
1640 sh	1680 sh	1220 w	1230 w	1.34	1.36					$\delta \text{H}_2\text{O}$

Table 2b: Main infrared OH stretching wavenumbers of H_3O^+ in non-stoichiometric beta alumina at 300K (after [42]). Oxygen atoms are labeled according the structure and the H-bond distance is extracted from the structure refinement.

Site	Crystal	Powder	Assignment	d O...O / nm
BR	3508 S	3508 S	vO-H...O _[5]	~0.287
mO	3495 m	3496 m	vO-H...O _[5]	~0.287
mO	-	3433 S	vO-H...O _[4]	~0.280
mO	3395 S	3395 S	vO-H...O _[5]	~0.280

all	1650 m		δ H ₂ O	
-----	--------	--	---------------------------	--

Table 2c: Main infrared OH stretching wavenumbers of H₅O₂⁺ and H₇O₃⁺ in beta alumina at 300K (after [42,151]), H₉O₄⁺ in isotopically diluted HUP and H₂O in isotopically diluted KUP at 300 and 130K (after [73,74]). The H-bond distance is given according to a 300K structure refinement (d).

H ₂ O 130K	H ₅ O ₂ ⁺ 300K	H ₇ O ₃ ⁺ 300K	H ₉ O ₄ ⁺		Assignment (d O...O / nm)
			130K	300K	
3493 S 3460 S 3400 S	3380 S (A-band)	3545 S	3380 S	3350 S	Terminal H ₂ O stretching, A-band (0.281)
	2900 S (B-band)	3235 S	3230 S		Terminal H ₃ O ⁺ stretching, B-band (0.269-0.271)
3290 S 3140 S	2540 S (C-band)	2880 S	3060 S		Central O-H...O mode, C-band (0.262)
1655 m	1700 sh 1650 m 1330 m 1100 w	1700 sh 1650 m 1330 m 1100 w	1780 S		Oxonium bending mode (v ₄) Water bending mode O-H-O ending mode Oxonium bending mode (v ₂)

Table 2d: Main incoherent inelastic neutron O-H peak wavenumbers of H₃O⁺ and H₅O₂⁺ in different proton conductors: hydrated and dehydrated beta aluminas [153,154], hydrated and dehydrated phosphotungstic acid [46] and jarosite [102].

Compound	Water Saturated beta alumina (H ₅ O ₂ ⁺)	beta alumina (H ₃ O ⁺ + H ₅ O ₂ ⁺)	Jarosite (H ₃ O ⁺)	PWA-6 H ₂ O (H ₅ O ₂ ⁺)	PWA-1 H ₂ O (H ₃ O ⁺)	PWA-0 H ₂ O (H ⁺)	Assignment
	150 280 460 550	140 280 460 550	103, 152 311 540	468 568	130,175 329 467	518 618	T'(H ₃ O ⁺) (H ₂ O) (H ₅ O ₂ ⁺) τ (H ₃ O ⁺) (H ₅ O ₂ ⁺)
	650 780	650 780	607 709	831	685		R(H ₃ O ⁺) τ (H ₃ O ⁺) (H ₅ O ₂ ⁺)
	980 1150 1380 1670	980 1150 1380 1670	1015 1722	1066 1735	1080 1660	1149	ν (H ⁺) ν ₂ (H ₃ O ⁺) ν ₄ (H ₃ O ⁺) 2 ν (H ⁺) 3 ν (H ⁺)
						2290 3340	

Raman analysis, especially of deuterated homologues, confirms the IR spectra, as usual but the number of observed bands is much smaller [42]. The assignments in Table 2 have been established taking into account the spectra after deuteration and comparison of the ν H/ ν D ratio. Indeed the isotopic ratio is different according to the type of movement and is with the polarization and the wave number a criterion of assignment of the modes of vibration.

Beta alumina appears as one of the solid networks allowing an oxonium ion to be particularly free of hydrogen bonding. Several interpretations are proposed to attribute the spectra. The symmetry of isolated oxonium ion is generally considered as C_{3v} but incoherent inelastic neutron spectroscopy data show that H_3O^+ actually has T_d symmetry at low temperature like the NH_4^+ ion due to the partial dynamic occupation of each T_d position by 3/4 of a proton. [153,154]

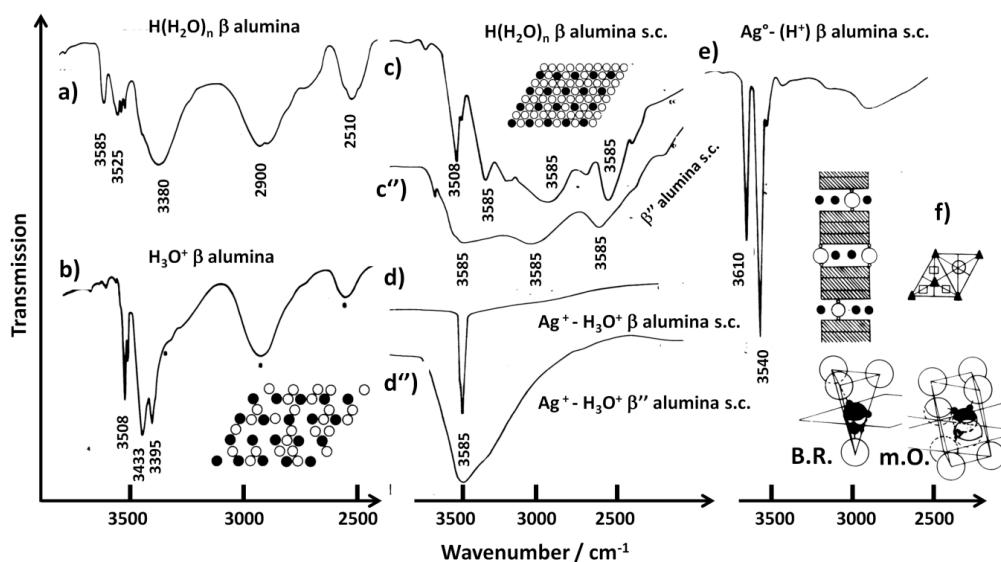


Figure 5. Infrared transmission spectra measured on beta and beta'' alumina single crystal along c axis (a,c,c'',d and e) and on a powder mull (b). A schematic of the structure is given in f); in c) the full occupation of the conducting plane by oxygen atoms of a water molecule and oxonium ions; in b) the partial occupation of the site; the different sites (Beever & Ross and anti-BR sites are indicated in f with black triangle; oxygen atom and middle-oxygen sites are indicated with open circle).

The peaks obtained at very high wavenumber for the mixed aluminate crystals of silver and "water" have been the subject of various interpretations. [81,155] Indeed, the exposure of silver aluminate single crystals in H_2 at ~ 770 K leads to the formation of Ag^0 clusters in the conduction planes of the single crystals and insertion of non-hydrated protons in the structure. The IR signature exhibits very fine peaks, close to 3540 and 3610 cm^{-1} (Figure 5e). The very high wavenumbers and the great narrowness of the peaks are proof of free O-H vibrators, without hydrogen bonding, probably thanks to the screening by silver nanoclusters. They are attributed to $(Al-O-)H^+$ species (which can be also written as $Al-(OH)^-$). It is likely that the observation of two peaks is to be linked to the existence of two types of Al-O-Al bridges, the normal bridge and the additional one located at the mO site to ensure the charge compensation arising from the non-stoichiometry.

The signatures of the OH^- , H_3O^+ and $H_5O_2^+$ species with the transition from fine peaks at very high wavenumbers to a signature consisting of wide bands ABC, is consistent with the initial descriptions of Hadzi et al. [57,58] and of Novak [51]: indeed, the modifications resulting from the strengthening

of hydrogen bonds displace the center of gravity of the ABC feature from about 3000 towards 2000 cm^{-1} and in rare cases up to 1000-800 cm^{-1} [51] and the ABC feature superimposes upon the modes of the network making it more difficult to observe of all the modes of the proton species. This example illustrates the potential offered by the combination of single crystal infrared analysis and partial ion exchange to isolate the ions in certain sites and facilitate the differentiation between the vibrational signatures of the ions according to the occupied site.

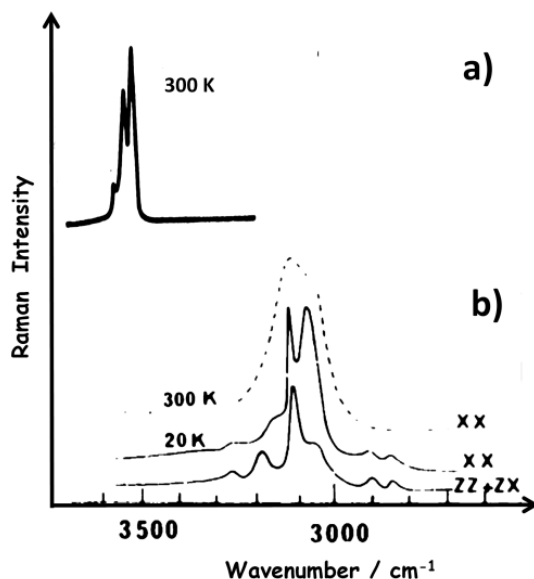


Figure 6. Raman spectrum recorded on oxonium (a) and ammonium (b) beta alumina single crystal for different polarizations at various temperatures (see text).

The Raman spectra of the proton species are always of weak intensity but the absence of other modes of variations in the range 3100-3800 cm^{-1} allows their observation. For instance, Figure 6 compares the Raman signatures of oxonium and ammonium ions in beta alumina. [13,42] Generally low site symmetry and distortion of the species causes g-u splitting (i.e. Raman - IR exclusion) to occur rarely and obtaining the infrared spectrum alone is sufficient to identify the proton species. The main advantage of Raman scattering is the better spectral resolution that allows the study of the shape variation with temperature without the need of isotopic dilution. Furthermore full measurement of polarized spectra is possible as shown in Figure 6 [13] which allows a precise description of the site and species symmetries.

3.1.3. Inelastic neutron scattering

Figure 7 shows the inelastic neutron vibration spectra for PWA at different hydration states corresponding to the species H_5O_2^+ ($\text{H}^+ 6\text{H}_2\text{O}$), H_3O^+ ($\text{H}^+ \text{H}_2\text{O}$) and H^+ ($\text{H}^+ 0.2 \text{H}_2\text{O}$) [43,46] as well as for

oxonium beta alumina and of the same compound saturated with water (H_5O_2^+). [153,154] Due to the anisotropy of beta alumina crystals (about 1 cm^2 platelet with $\sim 1 \text{ mm}$ thickness) and their common orientation in the aluminum cell with their c-axis perpendicular to the cell, the spectrum recorded by neutron spectroscopy correspond to that of a mosaic crystal of beta alumina .

As mentioned above, Keggin salts have many hydration states [153,154] while maintaining almost the same structure, which makes it possible to study structurally [43-45] and spectroscopically [44,46,53,70] the different protonic species. The INS spectra are characterized by defined peaks corresponding to the vibrational modes leading to a displacement of the proton and by a continuous background above $\sim 30\text{-}80 \text{ cm}^{-1}$. For comparison, the spectrum corresponding to the subtraction of the spectrum of oriented films of a polyaniline base (Emeraldine Base, a polymer whose aromatic rings have been deuterated so as not to contribute to the spectrum, as indicated above for beta alumina, orientation of the sample with lamellar structure is required to get 'nice' spectrum) by that of the same compound in the salt state (Emeraldine chloride salt: 2S) is shown. [143-145] The INS spectra of water-saturated and oxonium beta alumina crystals as well as simulations of the expected spectra for H_3O^+ and H_5O_2^+ are presented. [153,154] The first evidence is that, although the instrumental resolution is lower than that of IR instruments and degrades when the wavenumber increases, most of the peaks are much narrower than in infrared due to the absence of coupling. They are larger for PANI, a quasi amorphous polymer [143-145] than for beta alumina crystals.

The INS intensities being mainly a function of the amplitude of the movements of the hydrogen atoms and not to the dipole strength, the spectra are hardly comparable to the IR and Raman spectra but the INS spectra of compounds harboring similar species, namely H_5O_2^+ , H_3O^+ (Table 2d) are indeed rather similar regardless of the host network, due to the weak contribution of the elements of this framework: for instance, for H_3O^+ ion a translation mode around $130\text{-}150 \text{ cm}^{-1}$ as observed in Raman scattering [42,91-94], a libration mode around 450 cm^{-1} , deformation modes around $1100\text{-}1200 \text{ cm}^{-1}$ and 1650 cm^{-1} are obvious [91-94].

The INS spectrum obtained for the dehydrated PWA, but before the collapse of the Keggin salt structure into a tungsten bronze, i.e. for $\text{H}_3\text{PW}_{12}\text{O}_{40} \cdot 0.2\text{H}_2\text{O}$ composition, was unexpected: a strong ca. 1140 cm^{-1} peak and overtones at 2280 and 3400 cm^{-1} . Such a spectrum corresponds to that of an isolated harmonic oscillator, like a proton in its potential well, [46,156] in other words a proton free of covalent bond, hence an 'ionic' proton.

The other important and unexpected result is the importance of the background. In neutron scattering, this incoherent background is due to hydrogen atoms and its magnitude indicates that a significant number of the protons are not engaged in covalent bonds but delocalized. The mass of the

neutron is essentially the same as that of the proton. If a proton is not strongly bound in the lattice, recoil will shift the position of the mode and broaden the peak quite considerably. [153,154,156] This has been observed in all the proton conductors studied in my group and for some other compounds containing hydrogen such as the oxide forms of manganese and nickel oxides as well as carbons used as battery electrodes. [157-167] The interpretation that has been made is that ‘free’ protons form a proton gas or rather free polarons like electrons form a gas or polaron in some semiconductors. [3,11,62,168,169] More work is needed to better understand these species and their vibrational fingerprints.

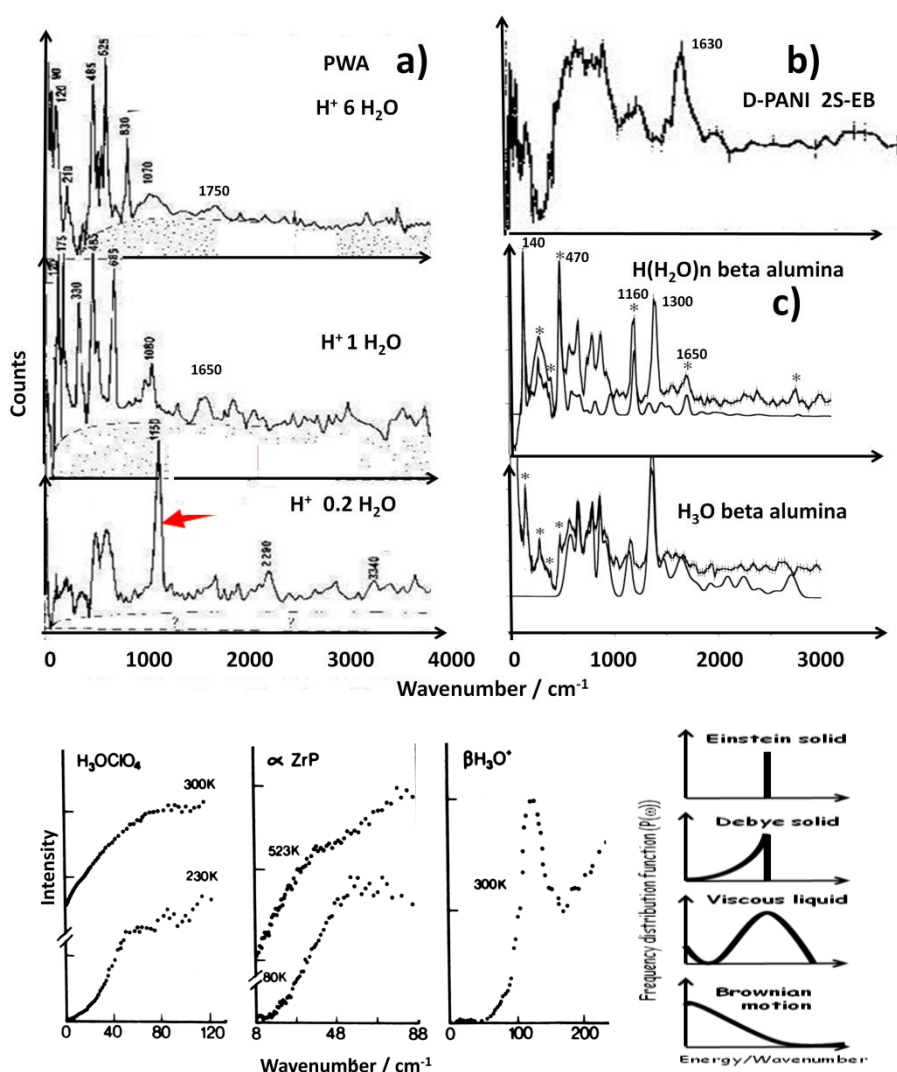


Figure 7. Comparison of the inelastic neutron scattering spectra recorded at low temperature (~ 30 K or lower) for $\text{H}_3\text{PW}_{12}\text{O}_{40} \cdot 6\text{H}_2\text{O}$, $\text{H}_3\text{PW}_{12}\text{O}_{40} \cdot \text{H}_2\text{O}$ and $\text{H}_3\text{PW}_{12}\text{O}_{40} \cdot 0.2\text{H}_2\text{O}$ powder (a), difference spectrum between ring-deuterated polyaniline ($\text{C}_6\text{D}_4\text{NH} \cdot \text{H}_2\text{O}$)_n emeraldine chloride and ($\text{C}_6\text{D}_4\text{NH} \cdot 0.25\text{H}_2\text{O}$)_n emeraldine base films at 30 K; (b) and $11 \text{Al}_2\text{O}_3 \cdot 1.3 [\text{H}(\text{H}_2\text{O})_2]\text{O}$ and $11 \text{Al}_2\text{O}_3 \cdot 1.3 [\text{H}_3\text{O}]\text{O}$ single crystals at 20 K (c); calculated spectra for H_3O_2^+ and H_3O^+ are given (solid line). Note the variable ‘background’. Details of the low wavenumber INS spectra are given for H_3OClO_4 , $\alpha \text{Zr}(\text{HPO}_4)$, H_2O and oxonium beta alumina.

The low wavenumber domain is also particularly informative (Figure 7). Indeed, as illustrated in the diagrams, the form of the vibrational excitation is very different depending on whether one has an isolated vibrator (Einstein solid), a set of coupled vibrators (Debye solid), a particle gas (Brownian motion) or a very viscous liquid for which a residence time can be considered [2,3,11,91-93]. Thus the INS spectrum of oxonium beta alumina (not very conductive at 300K) presents a fairly fine mode at $\sim 130 \text{ cm}^{-1}$, whereas for H_3OClO_4 at 300K and amorphous $\text{Zr}(\text{HPO}_4)_2 \cdot 6 \text{ H}_2\text{O}$ (aZrP) at 523 K, the temperature at which good conductivity and therefore proton diffusion is measured [91-93,101], the spectra show transition from a concave (Debye-like behavior) to convex curvature due to diffusive excitations as in viscous liquids.

3.2. Non-hydrated proton: *Nominally anhydrous phases*

Barium and strontium zirconate/cerate/titanate exhibit perovskite ABO_3 structure [170-175] and are studied since longtime – and use in many devices - because their dielectric and ferroelectric properties. Ideally the structure is cubic with A earth-alkali cations at the edges of the cube, oxygen atoms at the face centre and B cation at the centre of the cube. For symmetry reason no Raman spectrum is predicted for the cubic perovskite. Actually, ABO_3 structures are distorted into orthorhombic or tetragonal phase and oxygen vacancies are present. Partial substitution of zirconium with lanthanides (e.g. Y or Yb) or with atoms exhibiting different speciation (Ce, Ti) increases the vacancies number and the cell distortion.

Figure 8 compares the infrared spectra measured in transmission with an IR microscope for thin polished wafers (~ 100 to $150 \mu\text{m}$) of strontium zirconate densified at $\sim 94\%$ and 99% of the theoretical density [83] with those redrawn from the literature data [170-175] and with those powders of the carbonate and hydrated hydroxide of strontium [83]. The thermogravimetry spectra of the same samples are shown in Figure 7 (Note the different vertical scales) [83]. While practically no IR absorption is observed for the perfectly sintered ceramic apart from traces of carbonate at $\sim 1480 \text{ cm}^{-1}$, the ceramic densified at 94% of the theoretical density (which exceeds the densification of many ceramics in the literature) shows the same broad and fine bands as the powder of the hydrated strontium hydroxide left several days in the air to obtain its carbonation ($\sim 3590, 3500, 3400, 2950, 2350$ and 1700 cm^{-1}). The spectrum corresponds to the spectrum of hydroxyl groups free of H-bond (narrow peaks at 3500 cm^{-1} and above) associated to H-bonded species exhibiting A-B-C bands. The comparison with the IR spectra of the literature shows that what many authors have considered this fingerprint as characteristic of the bulk protonic species of perovskites are in fact

hydroxylated carbonate species localized on the surface or in the porosity of the samples. This interpretation had already been proposed in 1999 [170] before the analysis of dense polished ceramics demonstrated it (Figure 8). On the basis of these erroneous spectra, the hypothesis of formation of OH⁻ ions with strong hydrogen bonds leading to conduction by rocking and proton jumping was constructed [171]. The invalidity of this interpretation invalidates the hypothesis of a diffusion of the proton by jumping between close oxygen atoms. It is no doubt the simple nature of this hypothesis which gave it its large audience, still shared by many people. While the importance of performing conductivity measurements on a single crystal or on a perfectly dense ceramic (>95% of the theoretical density), in particular using a third electrode to eliminate surface conductivity, is well known to people studying electrodes and electrolytes to determine the reliable bulk value, the fact that this same criterion is capital in vibrational spectroscopy and in structural refinement studies of proton conductors is forgotten. It is symptomatic as we have already pointed out that the exact content of hydrogen element and water adsorbed on the surface of the material is often not determined in many studies. [6] On a powder, the quantity of protonated and/or hydrated species is all the more important if the powder is fine or if the sample is porous. Compounds rich in alkali and alkaline-earth carbonates can trap water and the species formed show intense infrared and Raman signatures.

The comparison of the Raman spectra of the ceramics before and after protonation under H₂O pressure (for economic reasons, energy production or conversion devices using gases must be pressurized, typically between 20 and 50 bars [11]) shows only weak modifications of the phonon spectrum (symetrization towards a more cubic structure [62,66] in agreement with the X-ray and neutron diffraction) [66,67,90,109] of the perovskite structure but with the addition of a strong fluorescence background. [62] Indeed, the perovskite structure accepts proton insertion due to the existence of oxygen ion vacancies created by the substitution of some Zr⁴⁺ (or Ce⁴⁺) ions by Ln (Y³⁺, Yb³⁺ or Er³⁺) ions for instance in the BaZr_{0.9}Ln_{0.1}O_{3-δ} (BZ:Ln) and SrZr_{0.9}Ln_{0.1}O_{3-δ} (SZ:Ln) compounds, studied and used as the ceramic membranes of electrolyzers [16,17] and CO₂ converters [19]. The main effect on the Raman fingerprint of protonation is the appearance of a wide fluorescence band which peaks around 2600 cm⁻¹ for green laser excitation. The phenomenon of fluorescence corresponds to slower (in the time scale the characteristic time is of the order of the 10⁻³ second to be compared of the 10⁻¹² second characteristic time of Raman scattering) but much more intense electronic transitions than Raman scattering. It results from electronic defects. These defects are not always identified. It can be assumed that the defects are due to particular interactions between the oxygen ion vacancies and the protons. A similar phenomenon has been observed for lanthanum silicate oxyapatites [176] which also have a non-stoichiometry in oxygen and can protonate. Note

that the autoclave protonation parameters influence the fluorescence intensity, more intense for protonation at 200-300°C (20 to 50 bars H₂O) than at 500-550°C (30 to 50 bars H₂O) [83].

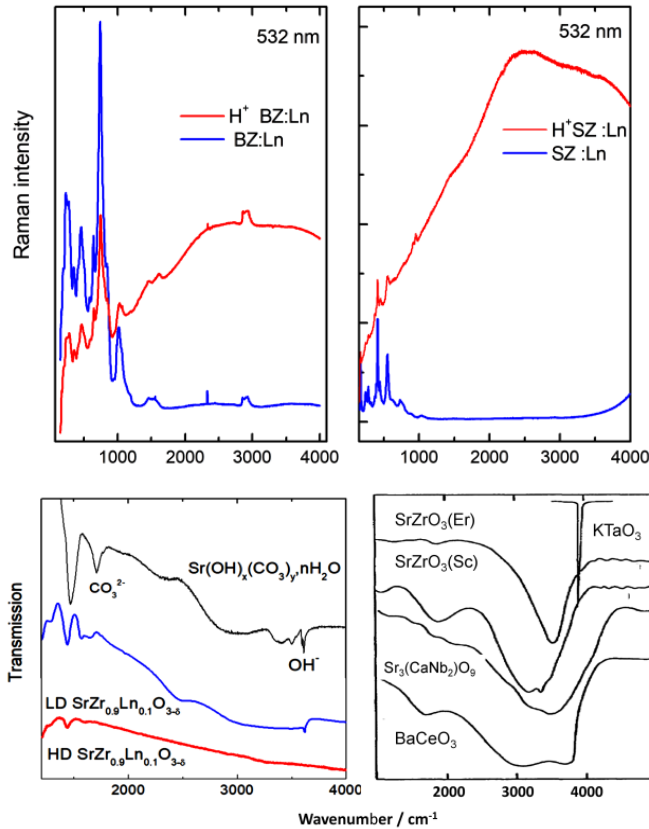


Figure 8. Top, comparison of Raman spectra measured on dense ceramic of barium zirconate (BZ, BaZr_{0.9}Y_{0.1}O_{3-δ}) and strontium zirconate (SZ, SrZr_{0.9}Y_{0.1}O_{3-δ}) before (blue) and after (red) protonation for several hours in autoclave at 200°C, 30 bar H₂O [60]; bottom, comparison of infrared spectra in transmission obtained for a powder of Sr(OH)_x(CO₃)_y·nH₂O (CsI pellet) and for polished thin ceramics perfectly densified (HD SrZr_{0.9}Er_{0.1}O_{3-δ}), densification ~99% theoretical density) and moderately densified (LD, ~94%) [83], dried at 300°C with spectra from the literature [170] of different perovskites.

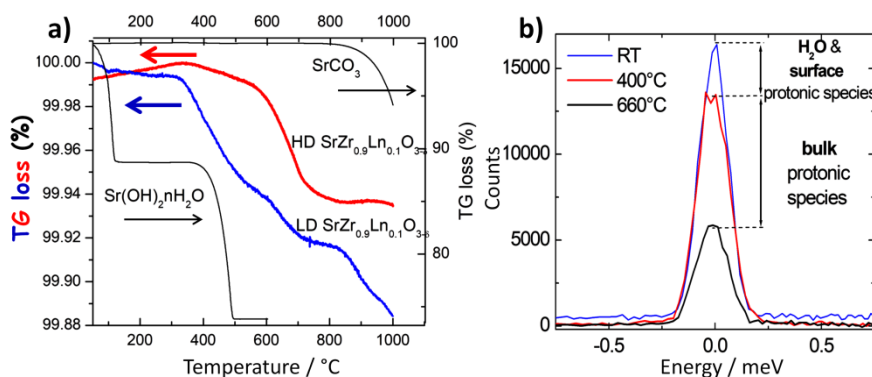


Figure 9. Comparison (a) of thermograms obtained for well-sintered (HD) and porous (LD) strontium zirconate ceramics (see Figure 6) with powder thermograms of strontium carbonate (SrCO_3) and hydroxide ($\text{Sr}(\text{OH})_2 \cdot n\text{H}_2\text{O}$); b) comparison of the elastic neutron scattering peaks measured for well-densified SZ:Yb ceramic pieces, at RT, at 400°C (under primary vacuum) and at 660°C (vacuum) [176].

The TGA curve of the ceramic at 94% densification (Figure 9) shows around 400°C a loss of mass identical to that of the hydroxide and around 900°C the loss of mass of the carbonate [83,177]. These phenomena are not observed for the dense ceramic which shows a loss of mass between 600 and 700°C, in conjunction with structural modifications [67,90,177]. The measurement of the elastic peak as a function of temperature [90] allows an accurate measurement of surface adsorbed water and bulk protons, for example $\text{SrZr}_{0.93}\text{Yb}_{0.07}\text{O}_{3-\delta}\text{H}_{0.004} \cdot 0.0008 \text{H}_2\text{O}$ for a ceramic densified at 99% and protonated at 500°C for 5 days under 80 bar H_2O . Similar information can be extracted from the plot of the background of the neutron diffraction pattern, the background being the incoherent scattering, in other words the elastic scattering measured on QENS instruments [90], see Figure 1.

We can see the experimental difficulty in studying the specific vibrational signatures of the protons of nominally anhydrous compounds. The small amount of proton in these materials makes it difficult to understand the dynamics of protons by neutron techniques because it is no longer possible to neglect the incoherent contribution of other elements. Attempts to measure the specific inelastic neutron signatures have been inconclusive, with practically no difference between the compound before and after protonation in the autoclave [177] except for the level of the continuous background that looks a little higher, but not so intense as that observed for PWA, beta alumina and PANI (Figure 7). It seems obvious that the background level is proportional to the H concentration which makes it difficult to study protonated perovskites.

Note, in the absence of significant H_2O pressure, the surface is preferentially affected. Also a number of authors who do not take any special experimental precautions, working on powders do not seek to separate the spectral contributions of bulk protons and surface species. This goes with little attention to the quality of densification of ceramics. The most clear modifications of the Raman spectrum of the perovskite phase caused by the insertion of protons concern the symmetrization already mentioned and the modifications of the sequence of the weak structural transitions between 300 and 700°C [67,90,177] and under hydrostatic pressure between 10 and 35 GPa. [178]

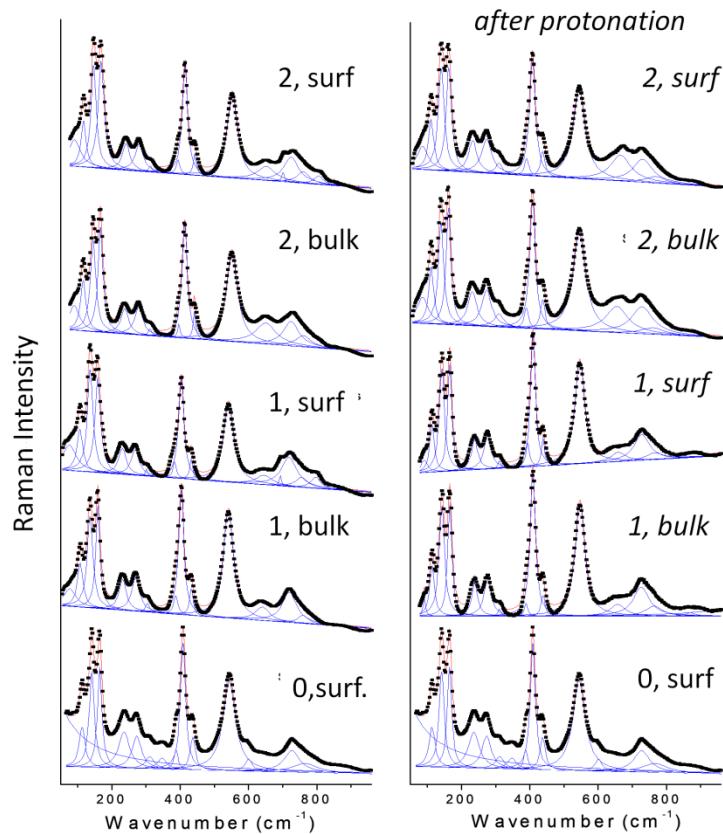


Figure 10. Left, comparison of the Raman spectra recorded on fragments of a $\text{SrZr}_{0.9}\text{Er}_{0.1}\text{O}_{3-\delta}$ 99% dense ceramic recorded on the surface (surf.) or on the centre of a fresh fracture (bulk) at room temperature as-sintered (0) and after a thermal treatment at 900°C under vacuum (1, first cycle; 2, second cycle); right, labels in italics: same samples after protonation at 500°C , 40 bar H_2O , for 5 days (composition $\text{SrZr}_{0.9}\text{Er}_{0.1}\text{O}_{3-\delta}\text{H}_{0.02}$) and after first and second heating cycle. The different vibrational modes are shown.

Figure 10 shows however the efficiency of Raman analysis to detect small structural changes induced by proton insertion. The compound is a highly densified ceramic (>95%) of strontium zirconate where 10% of the zirconium has been replaced by erbium to create oxygen vacancies. The Raman spectrum is characteristic of a perovskite with distortion of the ideally cubic lattice with a triplet below 200 cm^{-1} , and the intense modes of the modes of deformation (around 400 cm^{-1}) and elongation (around 550 cm^{-1}) of the ZrO_6 octahedron in a 'molecular' description of the Raman signature [62,178]. The partial substitution of zirconium ion by a cation with a lower charge (Y, Yb, Er or Ho) leads to the formation of an oxygen vacancy which results in a greater distortion of the lattice and an increase in the intensity of the Raman spectrum and the appearance - or a stronger intensity - of modes beyond 600 cm^{-1} , attributed to Zr-O stretching disturbed by the presence of substitution atoms and/or vacancies. The two spectra at the bottom of the figure were obtained on the sintered ceramic. The spectra above are obtained on the surface or after breaking on the core of the ceramic at RT after a first then a second firing cycle at 900°C under vacuum (the samples were also analyzed by neutron

diffraction)[178]. On the left the ceramic has not been protonated; on the right it was saturated with protons at 500°C under 40 bars of water vapor. We see the modifications of the vibration modes beyond 600 cm^{-1} which depend on the cycles, on the exposure to water and differ between core and surface, probably in relation to the surface-core gap gradient. The comparison of parameters and mesh volume also shows small differences in temperature behavior. Pressure analysis up to 40 GPa (under He in a diamond cell [178]) shows that protonation slightly shifts the phase transition temperatures. It is clear that given the few modifications measured on ceramics, studies on single crystals are essential to characterize the modifications induced by protonation on the vacancies, their state of charge and their organization.

Case study: post mortem study of the H-gradient in the perovskite electrolyte membrane after H₂ production

Obviously, the vibrational characterization of the protons inserted in the perovskite structure is difficult and uninformative by infrared spectroscopy. On the other hand, the importance of the fluorescence signal observed under green laser excitation allows one to collect important information on the existence of a protonation. This demonstrates the need to study the electronic defects associated with the formation of oxygen ion vacancies and the filling of some with oxygen from water molecules and the simultaneous incorporation of the two protons. Figure 11 shows the plot of the maximal intensity of fluorescence band measured on the fracture section of the electrolyte membrane extracted from the cell of a pressurized electrolyser having produced hydrogen for several tens of hours at 550°C. The fluorescence intensity is plotted from the anodic (exposed to pressurized H₂O, 30 bar) towards the cathodic side (producing hydrogen) of the fractured ceramic. Before fracture the membrane was characterized by impedance spectroscopy before and after operation: a variation in bulk resistivity is observed that demonstrated some modifications had occurred to the material. The fluorescence intensity (maximum around 2600 cm^{-1}) is constant for the first 0.4 mm then collapses. There is therefore a modification either of the proton content or of the nature of the proton and/or of its bond with the host lattice/oxygen vacancy. This is understandable because the ceramic membrane is subject to gradients of electric field and mobile species. Furthermore water pressure is maximal on the anodic side. Unfortunately the collection of this spectroscopic information requires the destruction of the ceramic membrane. Perhaps a pulsed laser beam – and therefore generating pulses intense enough to allow focusing at variable depth in a test device – could in the future avoid destructive analysis and operand analysis.

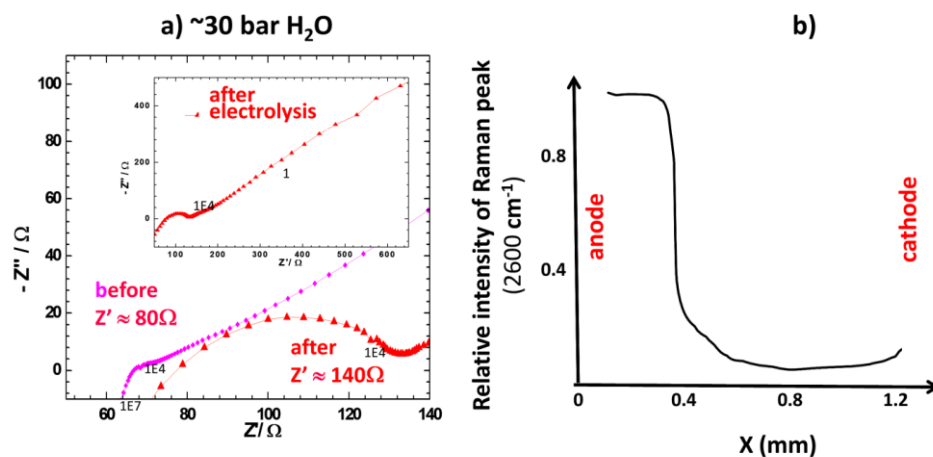


Figure 11. Comparison (a) of the impedance spectra at 550°C of a well-densified SZ:Ln ceramic membrane before and after several tens of hours of operation in an H₂O-air/H₂ pressurized electrolyser; b) evolution of the fluorescence signal at 2600 cm⁻¹ (green laser excitation) measured on the section (fracture) of the HD SZ:Ln membrane from the anodic face towards the cathodic face.

5. Conclusion

Infrared and Raman spectroscopies make it possible, with instruments whose cost is becoming lower, to obtain varied information concerning both the structure of the network hosting the proton species and the structure as well as the nature of the chemical bonds of the protonic species, in addition to their dynamic behavior. It appears obvious that infrared analysis is the most efficient method for oxonium and hydrated material if the preparation of the materials is possible and in particular if H/D isotopic dilution can be used to 'simplify' the spectrum and make it more informative on the site occupied by the proton species and the dynamic behavior of the proton. This is done at the cost of specific preparation and precise control of the samples: synthesis of pure samples, exposure to water vapor and equilibration, polishing and thin section preparation or 'fresh' fracture, etc. H/D isotopic substitutions and dilutions are essential. IR analysis is therefore very effective for compounds containing proton hydrates.

The short time of the light-matter interaction allows a dynamic view of the balance of species [53] that does not allow the diffraction of X-rays or neutrons. On the other hand, inelastic neutron scattering, although little used due to the large amount of sample mass required, and the limited number of sources and spectrometer(s) covering a large spectral window appears to be the most efficient method, but unfortunately spectra should be recorded at low temperature, therefore far from the state where the material develops its conductive properties. Quasi-elastic analyses and NMR are efficient methods for determining the dynamics of protons over all the temperature range, in particular at working temperature: activation energies of diffusive dynamics, jump distance, residence time and flight time, etc. Unfortunately the energy range covered by an instrument is very

limited and if the phenomenon does not occur with a characteristic energy close to that of the resolution of the instrument, the phenomenon disappears in the elastic peak or in the continuous background and escapes to measure.

Erroneous conclusions due to a lack of care in the elimination of surface species make it particularly difficult to study phases where the proton content is low and its conclusions are misleading if they are used to validate modeling and simulations. The observation of a continuous background on inelastic neutron spectra appears characteristic of proton conductors, but few teams have devoted themselves to these analyses and the progress of modeling and understanding remains slow.

Raman spectroscopy and the phenomena observed in association - fluorescence - is more effective for studying disturbances of the host network hosting proton species than for understanding proton species themselves. This makes it possible to establish the weak structural modifications also detectable by neutron diffraction. One of the main advantages is the possibility of working through an optical window and therefore of analyzing in situ surface modifications. Neutron methods that can be performed in aluminum alloy devices should allow for in situ measurements.

This review shows the variety and complexity of vibrational signatures as well as the importance of using single crystals to simplify spectra and attributions and avoid signal 'pollution' by surface species. It appears that the study and understanding of the properties of the inserted proton in nominally anhydrous oxides should have links to that of electronic defects and certainly requires the definition of new procedures.

Acknowledgments

As we have tried to prove, expertise in sample preparation and in carrying out measurements and their interpretation is decisive for vibrational analyses of proton conductors. Also the author would like to thank the experts who transmitted this know-how to him, in particular the late Dr Alexandre Novak, Dr André-Jean Dianoux and Professor Pierre Potier as well as the doctoral students, students and colleagues who contributed to the above work.

References

1. F. M. Ernsberger, The Nonconformist Ion, *J. Am. Ceram. Soc.* 66 (11) (1983) 747-750. <https://doi.org/10.1111/j.1151-2916.1983.tb10555.x>
2. P. Colomban, A. Novak, Proton transfer and superionic conductivity in solids and gels, *J. Mol. Struct.* 177 (1988) 277-308. [https://doi.org/10.1016/0022-2860\(88\)80094-2](https://doi.org/10.1016/0022-2860(88)80094-2)
3. P. Colomban (Ed.), *Proton Conductors: Solids, Membranes and Gel – Materials and Devices*, Cambridge University Press, Cambridge, United Kingdom, 1992.

4. A. Hérold, Une réflexion sur les éléments chimiques : leur division en quatre classes, *L'Actualité Chimique* 2011, 355, 52-54.
5. P. Atkins, J. A. Beran, *General Chemistry*, Scientific American Books, New York, USA, 1992.
6. P. Colomban, P. Proton and Protonic species: The Hidden Face of Solid State Chemistry. How to measure H-content in materials, *Fuel Cells* 13 (1) (2013) 6-18.
10.1002/fuce.201200088
7. W.T. Wilkins, A. Mateens, G.W. West, The Spectroscopic Study of Oxonium ions in Minerals, *Am. Miner.* 59 (1974) 811-819.
8. J. Bruinink, Proton migration in solids, *J. Appl. Electrochem.* 2 (1972) 239-249.
<https://link.springer.com/article/10.1007/BF02354982>
9. A. Potier, D. Rousselet, Conductivité électrique et diffusion du proton dans le perchlorate d'oxonium, *J. Chim. Phys. Phys.-Chim. Biol.* 70(6) (1973) 873-878.
DOI: <https://doi.org/10.1051/jcp/1973700873>
10. L. Glasser, Proton conduction and injection in solids, *Chem. Rev.* 75 (1975) 21-65.
<https://pubs.acs.org/doi/abs/10.1021/cr60293a002>
11. P. Colomban, Proton conductors and their applications: A tentative historical overview of the early researches, *Solid State Ionics* 334 (2019) 125-144.
<https://doi.org/10.1016/j.ssi.2019.01.032>
12. M.G. Shilton, A.T. Howe, Rapid H⁺ conductivity in hydrogen uranyl phosphate-A solid H⁺ electrolyte, *Mat. Res. Bull.* 12 (7) (1977) 701-706. [https://doi.org/10.1016/0025-5408\(77\)90129-5](https://doi.org/10.1016/0025-5408(77)90129-5)
13. P. Colomban, J.-P. Boilot, A. Kahn, G. Lucazeau, Structural investigation of protonic conductors: NH₄⁺ β alumina and stoichiometric H₃O⁺ β alumina, *Nouv. J. Chim.* 1978, 2(1), 21-33.
14. N. Baffier, J.C. Badot, P. Colomban, Conductivity of β" and ion-rich β-alumina. I. H⁺(H₂O)_n compounds, *Solid State Ionics* 2 (2) (1981) 107-113. [https://doi.org/10.1016/0167-2738\(81\)90006-0](https://doi.org/10.1016/0167-2738(81)90006-0)
15. N. Baffier, J.C. Badot, P. Colomban, Protonic conductivity of β" and ion-rich β-alumina- II Ammonium compounds, *Solid State Ionics* 13 (3) (1984) 233-236.
[https://doi.org/10.1016/0167-2738\(84\)90035-3](https://doi.org/10.1016/0167-2738(84)90035-3)
16. B. Sala, O. Lacroix, S. Willemin, K. Rhamouni, H. Takenouti, A. Van Der Lee, P. Goeriot, B. Bendjeriou, P. Colomban, Procédé d'optimisation de la conduction ionique d'une membrane conductrice ionique Patent WO 2008/152317 A2
17. B. Sala, O. Lacroix, S. Willemin, K. Rhamouni, H. Takenouti, A. Van der Lee, P. Goeriot, B. Bendjeriou, P. Colomban, Procédé d'optimisation de la conductivité assurée par le déplacement des protons H⁺ et/ou des ions OH⁻ d'une membrane conductrice, Patent EP2168198A2. <https://patents.google.com/patent/EP2168198A2>
18. F. Forrat, G. Dauge, P. Trévoux, G. Danner, M. Christen, Electrolyte solide a base de AlLaO₃ application aux piles à combustible, *C. R. Acad. Sci.* 259 (1964) 2813-2816.
<https://gallica.bnf.fr/ark:/12148/bpt6k4011c?rk=42918;4#> (accessed 2nd July 2022)
19. B. Sala, F. Grasset, O. Lacroix, A. Sirat, K. Rhamouni, M. Keddou, H. Takenouti, D. Goeriot, B. Bendjeriou, P. Colomban, A. Slodczyk, Pourcelly G., Van der Lee A., Sanchez J.G., Method for generating Hydrogen and Oxygen y steam electrolysis, Patent EP 12773302 A 20121011 (EP 2766512 A1 20140820 (FR) <https://data.epo.org/gpi/EP2766512A1>

20. M.L. Perry, T.F. Fuller, A historical perspective of fuel cell technology in the 20th century, *J. Electrochem. Soc.* 149(7) (2002) S59–S67.
<https://iopscience.iop.org/article/10.1149/1.1488651>
21. M. Marrony, *Proton Conducting Ceramics, from Fundamental to Applied Research*, Pan Stanford Publishing, Singapore, 2016.
22. Ph. Knauth, M.L. Di Vona, *Solid State Proton Conductors: Properties and Applications in Fuel Cells*, Wiley, New-York, 2012.
23. J. Beintema, On the composition and the crystallography of autunite and the meta-autunites, *Rec. Travaux Chim. Pays-Bas et Belgique*, 57 (2) (1938) 155-175.
<https://onlinelibrary.wiley.com/doi/abs/10.1002/recl.19380570206>
24. H. Saalfeld, H. Matthies, S.K. Datta, Ein neues Aluminiumoxidhydrat mit β Alumina Struktur, *Ber. Dtsch. Keram. Ges.* 45 (1968) 212-215.
25. M. Ross, H.T. Evans Jr, Studies of torbernite minerals (I). The crystal structure of abernathyite and structurally related compounds $\text{NH}_4(\text{UO}_2\text{AsO}_4) \cdot 3\text{H}_2\text{O}$ and $\text{K}(\text{H}_3\text{O})(\text{UO}_2\text{AsO}_4) \cdot 2.6\text{H}_2\text{O}$, *Am. Mineral.* 49 (11-12) (1964) 1578-1602.
<https://pubs.geoscienceworld.org/msa/ammin/article-abstract/49/11-12/1578/540005/Studies-of-the-torbernite-minerals-i-the-crystal?redirectedFrom=fulltext>
26. M. Ross, H.T. Evans Jr, Studies of Torbernite minerals (III). Role of interlayer oxonium potassium and ammonium ions, and water molecules, *Am. Mineral.* 1965, 50(1-2) (1965) 1-12. http://www.minsocam.org/msa/collectors_corner/amtoc/toc1965.htm
27. B. Morosin, Hydrogen Uranyl Phosphate tetrahydrate, A Hydrogen-ion solid electrolyte, *Acta Crystal. Section –Struct. Sci.* 34 (12) (1978) 3732-3734.
https://inis.iaea.org/search/search.aspx?orig_q=RN:10436776
28. Y.-F. Yu Yao, J.T. Kummer, Ion exchange properties of and rates of ionic diffusion in beta-alumina, *J. Inorg. Nucl. Chem.* 1967, 29(9) (1967) 2453–2475.
[https://doi.org/10.1016/0022-1902\(67\)80301-4](https://doi.org/10.1016/0022-1902(67)80301-4)
29. H. Bureau, C. Raepsaet, H. Khodja, A. Carraro, C. Aubaud, Determination of hydrogen content in geological samples using elastic recoil detection analysis (ERDA), *Geochim. Cosmochim. Acta* 73 (11) (2009) 3311–3322. <https://doi.org/10.1016/j.gca.2009.03.009>
30. R. Sundvall, R. Stalder, Water in upper mantle pyroxene megacrysts and xenocrysts: a survey study, *Am. Mineral.* 96 (8–9) (2011) 1215–1227.
<https://doi.org/10.2138/am.2011.3641>
31. D.G. Pearson, F.E. Brenker, F. Nestola, J. McNeill, L. Nasdala, M.T. Hutchison, S. Matveev, K. Mather, G. Silversmit, S. Schmitz, B. Vekemans, L. Vincze, Hydrous mantle transition zone indicated by ringwoodite included within diamond, *Nature* 507 (7491) (2014) 221–224.
<https://www.nature.com/articles/nature13080>
32. K. Funke, Solid state Ionics: from Michael Faraday to green energy—the European dimension, *Sci. Technol. Adv. Mater.* 14 (2013) 043502, <https://doi.org/10.1088/1468-6996/14/4/043502>.
33. W. van Gool (Ed.), *Fast Ion Transport in Solids, Solid State Batteries and Devices*, North-Holland/American Elsevier, Amsterdam, 1973.
34. J.T. Kummer, N. Weber, Battery having a molten alkali metal anode and a molten sulfur cathode, Ford Motor Co., Patent US3413150A, 1967.
<https://patents.google.com/patent/US3413150A/en>

35. G.D. Mahan, W.L. Roth, *Superionic Conductors*, Proc. Conf. on Superionic Conductors: Chemistry, Physic and Applications, Schenectady, 10th–12th May 1976, Plenum Press, New-York, 1976.
36. P. Vashishta, J.N. Mundy, G.K. Shenoy (Eds.), *Fast Ion Transport in Solids: Electrodes, and Electrolytes: Proceedings of the International Conference on Fast Ion Transport in Solids, Electrodes, and Electrolytes*, Lake Geneva, Wisconsin, U.S.A., May 21–25, 1979, North Holland, New York, 1979.
37. W.L. Roth, G.D. Mahan (Eds.), *Superionic Conductors*, Plenum Press, New York, 1976.
38. S. Geller (Ed.), *Solid Electrolytes*, Springer Verlag, Berlin, 1977.
39. P. Hagemuller, W. Van Gool (Eds.), *Solid Electrolytes*, Academic Press, New York, 1978
40. A. Clearfield (Ed.), *Inorganic Ion Exchange Materials*, CRC Press, Boca Raton, 1980.
41. <http://www.fuelcellstore.com/membranes/nafion>, Accessed date: June 2018.
42. P. Colomban, G. Lucazeau, R. Mercier, A. Novak, Vibrational spectra and structure of $H^+(H_2O)_n$ β -alumina, *J. Chem. Phys.* 67 (11) (1977) 5244-5251.
<https://doi.org/10.1063/1.434701>
43. U.B. Mioc, R.Z. Dimitrijevic, M. Davidovic, Z.P. Nedic, M.M. Mitrovic, P. Colomban, Thermally induced phase transformations of 12-tungstophosphoric acid 29-hydrate: synthesis and characterization of PW_8O_{26} -type bronzes, *J. Mater. Sci.* 29 (1994) 3705-3718.
<https://link.springer.com/article/10.1007/BF00357338>
44. A. Kremenovic, A. Spasojevic-de Bire, R. Dimitrijevic, P. Sciau, U.B. Mioc, Keggin's ion structural modification and expansion of dodecatungstophosphoric acid hexahydrate induced by temperature treatment: In situ X-ray powder diffraction and Raman investigations, *Solid State Ionics* 132 (1-2) (2000) 39-53. 10.1016/S0167-2738(00)00727-X
45. A. Kremenovic, A.S. Bire, F. Bouree, P. Colomban, R. Dimitrijevic, M. Davidovic, U.B. Mioc, Structural modifications of dodecatungstophosphoric acid hexahydrate induced by temperature in the 10-358 K range. In situ high-resolution neutron powder diffraction investigation, *Solid State Ionics* 150 (3-4) (2002) 431-442. 10.1016/S0167-2738(02)00419-8
46. U. Mioc, P. Colomban, M. Davidovic, J. Tomkinson, Inelastic neutron scattering study of protonic species during the thermal dehydration of 12-tungstophosphoric hexahydrate, *J. Mol. Struct.* 326 (1994) 99-107. [https://doi.org/10.1016/0022-2860\(94\)08345-2](https://doi.org/10.1016/0022-2860(94)08345-2)
47. L.I. Yeh, Y.T. Lee, J.T. Hougen, Vibration-Rotation spectroscopy of the hydrated hydronium ions $H_5O_2^+$ and $H_9O_4^+$, *J. Mol. Spectrosc.* 164 (2) (1994) 473-488.
<https://doi.org/10.1006/jmsp.1994.1090>
48. A. Potier, J.M. Leclercq, M. Allavena, SCF-LCGO calculations of the nonrigid structure of dioxonium ion – A basis for a structural analysis of $H_5O_2^+$ ion in crystals, *J. Phys. Chem.* 88 (6) (1984) 1125-1130. <https://pubs.acs.org/doi/abs/10.1021/j150650a019>
49. L. Angyan, M. Allavena, M. Picard, O. Tapia, A SCRF-CNDO/2 study on proton conductivity mechanisms in hydronium perchlorate – Towards a quantum chemical representation of defects and impurities in crystals, *J. Chem. Phys.* 77 (9) (1982) 4723-4733.
<https://doi.org/10.1063/1.444375>
50. A.L. Soolewski, W. Domcke, A Initio investigation of the structure and spectroscopy of hydronium-water cluster, *J. Phys. Chem. A.* 106 (16) (2002) 4158-4167.
<https://pubs.acs.org/doi/10.1021/jp013835k>

51. A. Novak, Hydrogen bonding in solids correlation of spectroscopic and crystallographic data, *Structure and Bonding*, 18 (1974) 177-216.
<https://link.springer.com/chapter/10.1007/BFb0116438>
52. A.L. McClellan, G.C. Pimentel, *Hydrogen Bond*, W.H. Freeman, San Francisco, 1960.
53. U. Mioc, M. Davidovic, N. Tjapkin, P. Colomban, A. Novak, Equilibrium of the protonic species in hydrates of some heteropolyacids at elevated temperatures, *Solid State Ionics* 46 (1-2) (1991) 103-109. [https://doi.org/10.1016/0167-2738\(91\)90136-Y](https://doi.org/10.1016/0167-2738(91)90136-Y)
54. P. Colomban, M. Pham Thi, A. Novak, Vibrational of phase transitions and conductivity mechanism in $\text{H}_3\text{OUO}_2\text{PO}_4 \cdot 3\text{H}_2\text{O}$ (HUP), *Solid State Comm.* 53 (9) (1985) 747-751.
[https://doi.org/10.1016/0038-1098\(85\)90212-1](https://doi.org/10.1016/0038-1098(85)90212-1)
55. J.C. Badot, Ph. Colomban, R-F & Microwave Dielectric Relaxations and Phase Transitions in Superionic Protonic Acid Sulphates (Selenates), *Solid State Ionics*, 35 (1-2) (1989), pp. 143-149.
56. Ph. Colomban, J.C. Badot, Frequency dependent conductivity and microwave relaxations in protonic conductors, *Solid State Ionics*, 61 (1-3) (1993), pp. 55-62.
57. D. Hadzi, Infrared spectra of strongly hydrogen bonded systems, *Pure Appl. Chem.* 11 (3-4) (1985) 435-454. <http://dx.doi.org/10.1351/pac196511030435>
58. D. Hadzi, S. Bratos, P. Schuster, G. Zundel, C. Sandorfy, Eds, *The Hydrogen bond*, North Holland: Amsterdam, 1976, ch2.
59. F. Fillaux, B. Marchon, A. Novak, J. Tomkinson, Proton dynamics in the hydrogen bond. Inelastic neutron scattering by single crystals of CsH_2PO_4 at 20 K, *Chem. Phys.* 130 (1-3) (1989) 257-270. [https://doi.org/10.1016/0301-0104\(89\)87055-7](https://doi.org/10.1016/0301-0104(89)87055-7)
60. M.P. Thi, M.H. HerzogCance, A. Potier, J. Potier, Vibrational spectroscopy study of the mixture $4\text{HNO}_3 \cdot \text{H}_2\text{O}$ in crystal, glassy and liquid states-Evidence of oxonium trihydrogentetranitrate, *J. Raman Spectrosc.* 11 (2) (1981) 96-107.
<https://doi.org/10.1002/jrs.1250110209>
61. P. Colomban, Hydrogen bonding in hydrogen-substituted lithium aluminosilicates, *J. Mol. Struct.* 270 (1992) 407-416. [https://doi.org/10.1016/0022-2860\(92\)85043-G](https://doi.org/10.1016/0022-2860(92)85043-G)
62. A. Slodczyk, Ph. Colomban, S. Willemin, O. Lacroix, B. Sala, Indirect Raman identification of the proton insertion in the high-temperature $[\text{Ba}/\text{Sr}][\text{Zr}/\text{Ti}]\text{O}_3$ -modified perovskite protonic conductors, *J. Raman Spectrosc.* 40 (5) (2009) 513-521. <https://doi.org/10.1002/jrs.2157>
63. F. Fillaux, Quantum entanglement and nonlocal proton transfer dynamics in dimers of formic acid and analogues, *Chem. Phys. Lett.* 408 (4-6) (2005) 302-306.
<https://doi.org/10.1016/j.cplett.2005.04.069>
64. F. Fillaux, A. Cousson, M.J. Gutmann, Proton transfer across hydrogen bonds: From reaction path to Schrödinger's cat, *Pure Appl. Chem.* 2007, 79 (6) (2007) 1023-1039.
<http://dx.doi.org/10.1351/pac200779061023>
65. S. Ikeda, S. Kashida, H. Sugimoto, Y. Yamada, S. Bennington, F. Fillaux, Inelastic neutron scattering study of the localized dynamics of protons in KHCO_3 single crystals, *Phys. Rev. B* 66 (18-1)(2002) 184302. <https://doi.org/10.1103/PhysRevB.66.184302>
66. A. Slodczyk, O. Zaafrani, M.D. Sharp, J.A. Kilner, B. Dabrowski, O. Lacroix, Ph. Colomban, Testing the chemical/structural stability of proton conducting perovskite ceramic membranes by in situ/ex situ autoclave Raman microscopy, *Membranes* 3 (4) (2013) 311-330. <https://doi.org/10.3390/membranes3040311>

67. P. Colomban, A. Slodczyk, The structural and dynamics neutron study of proton conductors: Difficulties and improvement procedures in protonated perovskite, *Eur. Phys. J.-Spec. Issue* 213 (1) (2012)171-193. [10.1140/epjst/e2012-01670-7](https://doi.org/10.1140/epjst/e2012-01670-7)
68. P. Kritzer, Corrosion in high-temperature and supercritical water and aqueous solutions: a review, *J. Supercritical Fluids* 29 (1-2) (2004), 1-29. [https://doi.org/10.1016/S0896-8446\(03\)00031-7](https://doi.org/10.1016/S0896-8446(03)00031-7)
69. G. Gouadec, P. Colomban, Raman Spectroscopy of nanomaterials: How spectra relate to disorder, particle size and mechanical properties, *Progr. Cryst. Growth & Character. Mater.* 53 (2007) 1-56. <https://doi.org/10.1016/j.pcrysgrow.2007.01.001>
70. U. B. Mioc, M.R. Todorovic, M. Davidovic, P. Colomban, I. Holclajtner-Antunovic, Heteropolycompounds-From Proton Conductors to Biomedical Agents, *Solid State Ionics*, 176 (39-40) (2005) 3005-3017. <https://doi.org/10.1016/j.ssi.2005.09.056>
71. V. Vendange, Ph. Colomban, Determination of the hydroxyl content in gels and porous 'glasses' from alkoxide hydrolysis by combined TGA and BET analysis, *J. Porous Mater.* 3 (1996) 193-200. <https://doi.org/10.1007/BF01134032>
72. T. Buffeteau, D. de Sousa Meneses, M. Dussauze, T. Tassaing, Spectroscopie infrarouge, in *Spectroscopies vibrationnelles. Théorie, aspects pratiques et applications*, G. Simon Ed., eac: Paris, 2020, pp 47-84. <https://hal.archives-ouvertes.fr/hal-03131715/>
73. M. PhamThi, P. Colomban, Vibrational study of $\text{H}_3\text{OUO}_2\text{PO}_4 \cdot 3\text{H}_2\text{O}$ (HUP) and related-compounds-Phase transitions and conductivity mechanisms: part I, $\text{KUO}_2\text{PO}_4 \cdot 3\text{H}_2\text{O}$ (KUP), *J. Phys. Chem. Solids* 46 (4) (1985) 493-504. [https://doi.org/10.1016/0022-3697\(85\)90118-0](https://doi.org/10.1016/0022-3697(85)90118-0)
74. M. PhamThi, P. Colomban, Vibrational study of $\text{H}_3\text{OUO}_2\text{PO}_4 \cdot 3\text{H}_2\text{O}$ (HUP) and related-compounds-Phase transitions and conductivity mechanisms: part II, $\text{H}_3\text{OUO}_2\text{PO}_4 \cdot 3\text{H}_2\text{O}$, *J. Phys. Chem. Solids* 46 (5) (1985) 565-578. [https://doi.org/10.1016/0022-3697\(85\)90219-7](https://doi.org/10.1016/0022-3697(85)90219-7)
75. M.P. Thi, Herzog J.F., M.H. HerzogCance, A. Potier, Dynamical aspects of a fast protonic conductor: Oxonium perchlorate: Part II. ^1H -NMR spin-lattice relaxation, *J. Mol. Struct.* 196 (1989) 291-305. [https://doi.org/10.1016/0022-2860\(89\)85026-4](https://doi.org/10.1016/0022-2860(89)85026-4)
76. M.H. Herzog-Cance, J. Potier, A. Potier, Study of motion and geometry of oxonium ion in crystallized salts using NMR-spectroscopy, *Advances Mol. Relax. & Interaction Processes* 14 (4) (1979) 245-267. DOI:10.1016/0378-4487(79)80010-2
77. M.H. Herzog-Cance, J. Potier, A. Potier, Wide line N.M.R. study of the proton hydrates in crystallized salts : III- di-aquooxonium ion, *Advances Mol. Relax. & Interaction Processes* 20 (3) (1981) 165-189. [https://doi.org/10.1016/0378-4487\(81\)80012-X](https://doi.org/10.1016/0378-4487(81)80012-X)
78. Ph. Colomban, G. Gouadec, Raman and IR micro-analysis of high performance polymer fibres tested in traction and compression, *Comp. Sci. Tech.* 69 (1) (2009) 10-16. <https://doi.org/10.1016/j.compscitech.2007.10.034>
79. P. Colomban, C. Doremieux-Morin, Y. Piffard, M.H. Limage, A. Novak, Equilibrium between protonic species and conductivity mechanisms in antimonic acid, $\text{H}_2\text{Sb}_4\text{O}_{11} \cdot n\text{H}_2\text{O}$, *J. Mol. Struct.* 213 (1989) 83-96. [https://doi.org/10.1016/0022-2860\(89\)85108-7](https://doi.org/10.1016/0022-2860(89)85108-7)
80. P. Colomban, M. Pham-Thi, A. Novak, Vibrational study of structures and phase transitions in caesium hydrogen selenate (CsHSeO_4), *J. Mol. Struct.* 161 (1987) 1-14. [https://doi.org/10.1016/0022-2860\(87\)85057-3](https://doi.org/10.1016/0022-2860(87)85057-3)
81. Ph. Colomban, Vibrational study of hydrogen beta alumina, *J. Phys. C.: Solid State Phys.* 14 (1985) 4325-4333. DOI:10.1088/0022-3719/14/29/020

82. P. Colomban, G. Lucazeau, Vibrational study of and conduction mechanisms in β alumina. I. Stoichiometric β alumina, *J. Chem. Phys.* 72 (1980) 1213-1224. <https://doi.org/10.1063/1.439264>
83. Ph. Colomban, O. Zaafrani, A. Slodczyk, Proton content and nature in Perovskite ceramic membrane for medium temperature fuel cells and electrolyzers, *Membranes* 2 (3) (2012) 493-509. <https://doi.org/10.3390/membranes2030493>
84. A. Gruger, A. Régis, T. Schmatko, P. Colomban, Nanostructure of Nafion® membranes at different states of hydration. An IR and Raman study, *Vibr. Spectrosc.* 26 (2) (2001) 215-225. [https://doi.org/10.1016/S0924-2031\(01\)00116-3](https://doi.org/10.1016/S0924-2031(01)00116-3)
85. P. Bawuah, J.A. Zeitler, Advances in terahertz time-domain spectroscopy of pharmaceutical solids: A review, *TRAC-Trends in Analytical Chem.* 139 (2021) 116272. <https://doi.org/10.1016/j.trac.2021.116272>
86. P.A. Egelstaff, *Thermal neutron scattering*, 1965, Academic Press.
87. M. Bee, *Quasi-elastic neutron scattering*, Adam Hilger, Bristol; 1985
88. S.W. Lovesey, *Theory of neutron scattering from condensed matter*, Vols. 1,2, Oxford University Press: Oxford, 1992.
89. G.J. Kearley, V.K. Peterson, Eds *Neutron applications in materials for energy*, *Neutron Scattering Applications and Techniques*, Springer, 2015. Doi: 10.1007/978-3-319-06656-1_1
90. Slodczyk, A., Colomban, P., André, G., Zaafrani, O., Grasset, F., Lacroix, O., Sala, B. Structural modifications induced by free protons in proton conducting perovskite zirconate membrane, *Solid State Ionics* 225 (SI) (2012) 214-218. 10.1016/j.ssi.2012.01.023
91. J.C. Lassègues, P. Colomban, Dynamical studies in solid ionic conductors by incoherent neutron scattering, in J. B. Goodenough, J. Jensen, M. Kleitz Eds, *Solid State Protonic Conductors II for Fuel Cells and Sensors*, Odensee University Press, Odensee, 1983, pp 201-213.
92. J.C. Lassègues, Incoherent neutron scattering studies of proton conductors: from the anhydrous solid state to aqueous solutions, in Ph. Colomban Ed. *Proton Conductors*, Cambridge University Press, Cambridge, 1992.
93. J.C. Lassègues, D. Cavagnat, Incoherent neutron scattering study of protonic conductors, *Physica B* 180-181 (Part 2) (1992) 645-650. [https://doi.org/10.1016/0921-4526\(92\)90422-O](https://doi.org/10.1016/0921-4526(92)90422-O)
94. J.C. Lassègues, M. Fouassier, N. Baffier, P. Colomban, A.J. Dianoux, Neutron scattering study of the proton dynamics in NH_4^+ and OH_3^+ β alumina, *J. Physique* 41 (3) (1980) 273-280. <https://doi.org/10.1051/jphys:01980004103027300>
95. J.D. Axe, L.M. Corliss, J.M. Hasting, W.L. Roth, O. Muller, Neutron scattering study of NH_4^+ Motion in NH_4^+ β -alumina, *J. Phys. Chem. Sol.* 39 (2) (1978) 155-159. [https://doi.org/10.1016/0022-3697\(78\)90216-0](https://doi.org/10.1016/0022-3697(78)90216-0)
96. T. Springer, *Molecular Rotations and Diffusion in Solids*, in *Particular Hydrogen in Metals*, in *Dynamics of Solids and Liquids by neutron scattering*, S.W. Lovesey, T. Springer Eds, TCPHY, vol. 3, Springer-Verlag, Berlin, 1977, p255-300.
97. A.J. Dianoux, *Quasi-Elastic and Inelastic Neutron Scattering*, ch. In *The Time Domain in Surface and Structural Dynamics*, G.J. Long, F. Grandjean (eds), NATO ASI Series, vol. 228, Springer, Dordrecht, pp. 179-212. https://doi.org/10.1007/978-94-009-2929-6_10

98. T. Springer, R. E. Lechner, Diffusion Studies of Solids by Quasielastic Neutron Scattering, ch 3, Heitjans, P., Kärger, J. (eds) Diffusion in Condensed Matter. Springer, Berlin, Heidelberg, 2005. DOI: [10.1007/3-540-30970-5_3](https://doi.org/10.1007/3-540-30970-5_3)
99. C. Poinignon, A. Fitch, .E.F. Fender, Proton motions in $\text{H}_2\text{O}_2\text{PO}_4 \cdot 3\text{H}_2\text{O}$ (HUP) by quasielastic neutron-scattering, Solid State Ionics 9-10 (1983) 1049-1054. [https://doi.org/10.1016/0167-2738\(83\)90129-7](https://doi.org/10.1016/0167-2738(83)90129-7)
100. C. Poinignon, The use of quasielastic neutron-scattering to study the mechanism of proton-transfer in fast solid proton conductors, Solid State Ionics 35(1-2) (1989) 107-113. [https://doi.org/10.1016/0167-2738\(89\)90019-2](https://doi.org/10.1016/0167-2738(89)90019-2)
101. M.P. Thi, J.F. Herzog, M.H. Herzog-Cance, A. Potier, C. Poinignon, Dynamic aspects of a fast protonic conductor – Oxonium perchlorate. Part I. Raman and Inelastic neutron scattering spectra, J. Mol. Struct. 195 (1989) 293-310. [https://doi.org/10.1016/0022-2860\(89\)80176-0](https://doi.org/10.1016/0022-2860(89)80176-0)
102. D.J. Jones, J. Rozière, Complementary of optical and incoherent inelastic neutron-scattering spectroscopies in the study of conducting materials, Solid State Ionics 61 (1-3) (1993) 13-22. [10.1016/0167-2738\(93\)90329-2](https://doi.org/10.1016/0167-2738(93)90329-2)
103. P. Colomban, A. Novak, Nature of the protonic species and the gel-crystal transition in hydrated zirconium phosphate, J. Mol. Struct. 198 (1989) 277-295. [https://doi.org/10.1016/0022-2860\(89\)80044-4](https://doi.org/10.1016/0022-2860(89)80044-4)
104. P. Colomban, J.C. Lassègues, A. Novak, M. Pham Thi, C. Touret-Poinignon, Superionic Protonic Conductor CsHSO_4 , Studies in Physical and Theoretical Chemistry N°46, Proc. Dynamics of Molecular Crystal, J. Lascombe Ed., 1986, Elsevier: Amsterdam, pp 277-283.
105. P. Colomban, M. Pham-Thi, A. Novak, Influence of thermal and mechanical treatment and of water on structural phase transitions in CsHSO_4 , Solid State Ionics 24 (3) (1987) 193-203. [https://doi.org/10.1016/0167-2738\(87\)90160-3](https://doi.org/10.1016/0167-2738(87)90160-3)
106. D.A. Long, Raman Spectroscopy, McGraw Hill, 1977.
107. L.S. Taylor, F.W. Langkilde, G. Zograf, Fourier Transform Raman spectroscopic study of the interaction of water vapor with amorphous polymers, J. Pharm. Sci. 90(7) (2001) 888-901. DOI: [10.1002/jps.1041](https://doi.org/10.1002/jps.1041)
108. A. Mineshige, S. Okada, M. Kobune, T. Yazawa, Monitoring of water dissolution into high temperature protonic conductors, Solid State Ionics 178 (7-10) (2007) 713-715. <https://doi.org/10.1016/j.ssi.2007.02.032>
109. A. Slodczyk, M.D. Sharp, S. Upasen, P. Colomban, J.A. Kilner, Combined bulk and surface analysis of the $\text{aCe}_{0.5}\text{Zr}_{0.3}\text{Y}_{0.16}\text{Zn}_{0.04}\text{O}_{3-d}$ (CZY) ceramic proton-conducting electrolyte, Solid State Ionics 262 (2014) 870-874. <https://doi.org/10.1016/j.ssi.2013.12.044>
110. G. Simon, L. Meziane, A. Courty, P. Colomban, I. Lisiecki, Low wavenumber Raman scattering of cobalt nanoparticles self-organized in 3D superlattices far from surface Plasmon resonance, J. Raman Spectrosc. 47 (2) (2015) 248-251. <https://doi.org/10.1002/jrs.4782>
111. K. Abiko, Y. Kato, H. Hohjo, Y. Kishida, E. Sudo, Raman imaging of residual stress distribution in epoxy resin and metal interface, J. Raman Spectrosc. 51(1) (2020) 193-200. <https://doi.org/10.1002/jrs.5756>
112. Ph. Colomban, G. Gouadec, J. Mathez, J. Tschember, P. Pérès, Raman stress measurement in opaque Cf/epoxy composites submitted to tensile strain, Composites: Part A 37 (4) (2006) 646-651. <https://doi.org/10.1016/j.compositesa.2005.05.004>

113. Ph. Colomban, Understanding the nano- and macromechanical behaviour, the failure and fatigue mechanisms of advanced and natural polymer fibres by Raman/IR microspectrometry, *Adv. Nat. Sci. Nanosci. Nanotechnol.* 4 (1) (2013) 013001. <https://iopscience.iop.org/article/10.1088/2043-6262/4/1/013001>
114. U. Lavrencic Stangar, B. Orel, A. Surca Vuk, G. Sagon, Ph. Colomban, E. Stathatos, P. Lianos, In situ Resonance Raman microspectroscopy of a solid-state dye-sensitized photoelectrochemical cell, *J. Electrochem. Soc.* 149 (11) (2002) E413-E423. <https://iopscience.iop.org/article/10.1149/1.1509071/meta>
115. A. Surca Vuk, M. Gaberscek, B. Orel, Ph. Colomban, In situ Resonance Raman spectroelectrochemical studies of a semisolid redox (I_3^-/I^-) electrolyte encapsulated in a Hybrid electrochromic cell, *J. Electrochem. Soc.* 151(4) (2004) E150-E161. <https://iopscience.iop.org/article/10.1149/1.1649750/meta>
116. P. Lenfant, D. Plass, M. Ruffo, P. Colomban, J.P. Boilot, Céramiques d'alumine β et de ferrite β pour sonde à protons, *Mater. Res. Bull.* 15 (12) (1980) 1817-1827. [https://doi.org/10.1016/0025-5408\(80\)90202-0](https://doi.org/10.1016/0025-5408(80)90202-0)
117. P. Schnell, G. Velasco, P. Colomban, β -alumina-like thin film, *Solid State Ionics* 5 (1981) 291-294. [https://doi.org/10.1016/0167-2738\(81\)90250-2](https://doi.org/10.1016/0167-2738(81)90250-2)
118. J.P. Schnell, G. Velasco, D. Dubreuil, D. Dieumegard, M. Croset, P. Colomban, Hydrogenated β -alumina-like thin films, *Solid State Ionics* 9 & 10 (1983) 1465-1468. [https://doi.org/10.1016/0167-2738\(83\)90196-0](https://doi.org/10.1016/0167-2738(83)90196-0)
119. R. Collongues, D. Gourier, A. Kahn, J.P. Boilot, P. Colomban, A. Wicker, β alumina, a typical solid electrolyte: Latest developments in fundamental approach and in battery utilization, *J. Phys. Chem. Solids* 45 (10) (1984) 981-1013. [https://doi.org/10.1016/0022-3697\(84\)90045-3](https://doi.org/10.1016/0022-3697(84)90045-3)
120. C.J. Howard, K.S. Knight, B.J. Kennedy, E.H. Kisi, The structural phase transitions in strontium zirconate revisited, *J. Phys. Condens. Matter* 12, L677 (2000). <https://iopscience.iop.org/article/10.1088/0953-8984/12/45/101>
121. K.S. Knight, Powder neutron diffraction studies of $BaCe_{0.9}Y_{0.1}O_{2.95}$ and $BaCeO_3$ at 4.2K: a possible structural site for the proton, *Solid State Ionics* 127 (1-2) (2000) 43-48. [https://doi.org/10.1016/S0167-2738\(99\)00269-6](https://doi.org/10.1016/S0167-2738(99)00269-6)
122. I. Sosnowska, R. Przenioslo, W. Schafer, W. Kockelmann, R. Hempelmann, K. Wysocki, Possible deuterium positions in the high-temperature deuterated proton conductor on $Ba_3Ca_{1+y}Nb_{2-y}O_{9-\delta}$ studied by neutron and X-ray powder diffraction, *J. Alloys Compd.* 328 (1-2) (2001) 226-230. [https://doi.org/10.1016/S0925-8388\(01\)01299-3](https://doi.org/10.1016/S0925-8388(01)01299-3)
123. J.S. Bae, W.K. Choo, Ch.H. Lee, The crystal structure of $Ba(Ce_{0.8}Zr_{0.2})O_3$, *J. Eur. Cer. Soc.* 21 (10-11) (2001) 1779-1782. [https://doi.org/10.1016/S0955-2219\(01\)00114-5](https://doi.org/10.1016/S0955-2219(01)00114-5)
124. K. Oikawa, T. Kamiyama, S. Ikeda, T. Shishido, S. Yamaguchi, Neutron powder diffraction studies on $Ba_3Ca_{1+x}Nb_{2-x}O_{9-3x/2}$ complex perovskite-type oxides, *Solid State Ionics* 154-155 (2002) 641-646. [https://doi.org/10.1016/S0167-2738\(02\)00511-8](https://doi.org/10.1016/S0167-2738(02)00511-8)
125. I. Ahmed, S.G. Eriksson, E. Ahlberg, C.S. Knee, M. Karlsson, A. Matic, D. Engberg, L. Börjesson, Proton conductivity and low temperature structure of In-doped $BaZrO_3$, *Solid State Ionics* 177 (26-32) (2006) 2357-2362. <https://doi.org/10.1016/j.ssi.2006.05.030>
126. I. Ahmed, S.G. Eriksson, A. Ahlberg, C.S. Knee, H. Götlind, L.G. Johansson, M. Karlsson, A. Matic, L. Börjesson, Structural study and proton conductivity in Y-doped $BaZrO_3$, *Solid State Ionics* 178 (7-10) (2007) 515-520. <https://doi.org/10.1016/j.ssi.2006.11.011>

127. A.K. Azad, J.T.S. Irvine, High density and low temperature sintered of proton conductor $\text{BaCe}_{0.5}\text{Zr}_{0.35}\text{Sc}_{0.1}\text{Zn}_{0.05}\text{O}_{3-\delta}$, *Solid State Ionics* 179(19-20) (2008) 678-682. <https://doi.org/10.1016/j.ssi.2008.04.036>
128. I. Ahmed, C.S. Knee, M. Karlsson, S.G. Eriksson, P.F. Henry, A. Matic, D. Engberg, L. Börjesson, Location of deuteron sites in the proton conducting perovskite $\text{BaZr}_{0.50}\text{In}_{0.50}\text{O}_{3-y}$, *J. Alloys Compd.* 450 (1-2) (2008) 103-110. <https://doi.org/10.1016/j.jallcom.2006.11.154>
129. T. Shimoyama, T. Tojo, H. Kawaji, T. Atake, N. Igawa, Y. Ishii, Determination of deuterium location in $\text{Ba}_3\text{Ca}_{1.18}\text{Nb}_{1.82}\text{O}_{8.73}$, *Solid State Ionics* 179 (7-8) (2008) 231-235.
130. T. Shimoyama, T. Tojo, H. Kawaji, T. Atake, H. Fukazawa, N. Igawa, Crystal structure and lattice vibration of proton dissolved $\text{BaZr}_{0.8}\text{Sc}_{0.2}\text{O}_{2.9}$, *Solid State Ionics* 180 (6-8) (2009) 560-562.
131. M. Karlsson, Neutron Scattering of Proton-Conducting Ceramics, In: Kearley, G., Peterson, V. (eds), *Neutron Applications in Materials for Energy, Neutron Scattering Applications and Techniques*. Springer, Cham, Swiss, pp 243-271. https://doi.org/10.1007/978-3-319-06656-1_9
132. P. Teulon, J. Rozière, Synthesis and crystal-structure of $[\text{H}_5\text{O}_2][\text{Ru}(\text{CO})_3\text{Cl}_3]\cdot\text{SbCl}_3$, *Zeit; Anorg. & Allg. Chem.* 1981, 483(12), 219-224. 10.1002/zaac.19814831226
133. J. Majzlan, R. Stevens, J. Boerio-Goates, B.F. Woodfield, A. Navrotsky, M.K. Crawford, T.G. Amos, Thermodynamic properties, low-temperature heat-capacity anomalies, and single-crystal X-ray refinement of hydronium jarosite $(\text{H}_3\text{O})\text{Fe}^{3+}(\text{SO}_4)_2(\text{OH})(6)$, *Phys. & Chem. Miner.* 2004, 31(8), 518-531.
134. R.M. Bolanz, J. Gottlicher, R. Steininger, A. Wiczorek, Structural incorporation of As^{5+} into rhomboclase $(\text{H}_5\text{O}_2)\text{Fe}^{3+}(\text{SO}_4)_2$ center dot $2\text{H}_2\text{O}$ and $(\text{H}_3\text{O})\text{Fe}(\text{SO}_4)_2$, *Chemosphere* 2016, 146, 338-345.
135. D. Banerjee, A.M. Plonka, S.J. Kim, W.Q. Xu, J. B. Parise, Synthesis, structural characterization and high pressure phase transitions of monolithium hydronium sulfate, *J. Solid State Chem.* 2013, 197, 181-185.
136. M. Catti, R.M. Ierson, Order-disorder of the hydronium ion and low-temperature phase transition of $(\text{H}_3\text{O})\text{Zr}_2(\text{PO}_4)_3$ NASICON by neutron diffraction, *J. Chem. Phys. Chem.* 2002, 106(46), 11916-11921.
137. J.A. Alonso, X. Turrillas, Location of H^+ sites in the fast proton-conductor $(\text{H}_3\text{O})\text{SbTeO}_6$ pyrochlore, *Dalton Trans.* 2005, 5, 865-867.
138. G. Picotin, J. Rozière, J. Potier, A. Potier, Vibrational spectroscopy of dehydrates of complex acids HSbCl_6 , HGaCl_6 , HGaCl_4 , HGaBr_4 – Study of free H_5O_2^+ ions, *Adv. Mol. Relax. Proc.* 1975, 7(3), 177-188. 10.1016/0001-8716(75)80024-1
139. M. Volmer, The existence of oxonium-perchlorate, *Justus Liebigs Ann. Chem.* 1924, 440, 200-202
140. R. Minkwitz, S. Schneider, A. Kornath, On the reaction of phosphorous acid with superacids and the crystal structure of $\text{H}_5\text{O}_2^+\text{SbF}_6^-$ and $\text{Me}_4\text{N}^+\text{HPF}_6^-$, *Inorg. Chem.* 1998, 37, 18, 4662–4665. <https://doi.org/10.1021/ic971252c>
141. Sanjuan, M.L., Orera, A., Sobrados, I., Fuentes, A.F., Sanz, J. Structural transition in orthorhombic $\text{Li}_{5-x}\text{H}_x\text{La}_3\text{Nb}_2\text{O}_{12}$ garnets induced by a concerted lithium and proton diffusion mechanism, *J. Mater. Chem. A* 2018, 6(6), 2708-2720. DOI:10.1039/c7ta10431f

142. Kumar, B.V., Velchurri, R., Prasad, G., Vithal, M. Preparation, characterization, spectral and conductivity studies of $\text{Na}_3\text{MgZr}(\text{PO}_4)_3$ and $\text{Na}_{0.1}(\text{H}_3\text{O})(2.9)\text{MgZr}(\text{PO}_4)_3$, *Ceram. Int.* 2009, 35(7), 2719-2725. Doi:10.1016/j.ceramint.2009.03.009
143. P. Colomban, A. Gruger, A. Novak, A. Régis, Infrared and Raman study of polyaniline Part I. Hydrogen bonding and electronic mobility in emeraldine salts, *J. Mol. Struct.* 317 (1994) 261-267. [https://doi.org/10.1016/0022-2860\(93\)07898-7](https://doi.org/10.1016/0022-2860(93)07898-7)
144. R. Baddour-Hadjean, F. Fillaux, P. Colomban, A. Gruger, A. Régis, S.F. Parker, Inelastic neutron scattering study of proton dynamics in polyanilines, *Synth. Metals* 81 (1996) 211-214. [https://doi.org/10.1016/S0379-6779\(96\)03750-2](https://doi.org/10.1016/S0379-6779(96)03750-2)
145. F. Fillaux, N. Leygue, R. Baddour-Hadjean, S. Parker, P. Colomban, A. Gruger, A. Régis, L.T.L. Yu, Inelastic neutron scattering studies of polyanilines and partially deuterated analogues, *Chem. Phys.* 216 (1997) 281-293. [https://doi.org/10.1016/S0301-0104\(96\)00382-5](https://doi.org/10.1016/S0301-0104(96)00382-5)
146. A. Potier, D. Rousselet, Electric-Conductivity and Protonic Diffusion in Oxonium Perchlorate, *J. Chim. Phys. Phys.* 70 (6) (1973) 873-878. DOI: 10.1051/jcp/1973700873
147. A.T. Howe, H. Sheffield, P.E. Childs, M.G. Shilton, Fabrication of films of Hydrogen Uranyl Phosphate Tetrahydrate and their use as electrochromic displays, *Thin Solid Films* 67 (2) (1980) 365-370. [https://doi.org/10.1016/0040-6090\(80\)90471-X](https://doi.org/10.1016/0040-6090(80)90471-X)
148. M. Pham Thi, G. Velasco, P. Colomban, Percolation Threshold in a HUP/C Double Layer Supercapacitor, *J. Mater. Sci. Letts.* 5 (1986) 415-417. <https://doi.org/10.1007/BF01672346>
149. Benisty H., Colomban P. Chazalviel J.-N., Electron Accumulation Layer at n-Si / non-liquid Electrolyte Interfaces, *Appl. Phys. Lett.* 51 (14) (1987) 1121-1123. <https://doi.org/10.1063/1.98759>
150. P. Lenfant, D. Plas, M. Ruffo, J.-P. Boilot, P. Colomban, Céramiques d'alumine β et de ferrite β pour sonde à protons, *Mat. Res. Bull.* 15, 1817-1827 (1980). [https://doi.org/10.1016/0025-5408\(80\)90202-0](https://doi.org/10.1016/0025-5408(80)90202-0)
151. P. Colomban, A. Novak, Protonic Species, Conductivity and Vibrational Spectra of β/β'' Aluminas, *Solid State Ionics* 5, 241-244 (1981). [https://doi.org/10.1016/0167-2738\(81\)90238-1](https://doi.org/10.1016/0167-2738(81)90238-1)
152. P. Colomban, Raman Study of the Formation of Transition Alumina Single Crystal from Protonic β/β'' Aluminas, *J. Mater. Sci. Lett* 7 (1988) 1324-1326. <https://doi.org/10.1007/BF00719972>
153. P. Colomban, F. Fillaux, J. Tomkinson, G.J. Kearley, Proton dynamics in β alumina, *Physica B* 213 (1995) 634-636. [https://doi.org/10.1016/0921-4526\(95\)00234-Z](https://doi.org/10.1016/0921-4526(95)00234-Z)
154. P. Colomban, F. Fillaux, J. Tomkinson, G.J. Kearley, Inelastic neutron scattering study of proton dynamics in β alumina, *Solid State Ionics* 77 (1995) 45-50. [https://doi.org/10.1016/0167-2738\(94\)00259-U](https://doi.org/10.1016/0167-2738(94)00259-U)
155. W. Hayes, L. Holden, B.C. Tofield, *J. Phys. C: Solid State Phys.* 13 (1980) 4217-4227. <https://iopscience.iop.org/article/10.1088/0022-3719/13/22/016/pdf> (accessed 2nd July 2022)
156. P. Colomban, J. Tomkinson, Novel forms of hydrogen in solids : the ionic proton and the "free" proton, *Solid State Ionics* 97 (1997) 123-134. [https://doi.org/10.1016/S0167-2738\(97\)00046-5](https://doi.org/10.1016/S0167-2738(97)00046-5)

157. F. Fillaux, H. OuBoumour, J. Tomkinson, L.T. Yu, An Inelastic neutron-scattering study of the proton dynamics in Gamma-MnO₂, *Chem. Phys.* 149 (3) (1991) 459-469. [https://doi.org/10.1016/0301-0104\(91\)90045-U](https://doi.org/10.1016/0301-0104(91)90045-U)
158. F. Fillaux, CH Cachet, H. Ououmour, J. Tomkinson, C. LevyClement, L.T. Yu, Inelastic neutron-scattering study of the proton dynamics in manganese oxides. 1. Gamma-MnO₂ and manganite, *J. Electrochem. Soc.* 140 (3) (1993) 585-591. <https://iopscience.iop.org/article/10.1149/1.2056125>
159. F. Fillaux, R. Papoular, A. Lautié, J. Tomkinson, Inelastic neutron-Scattering study of free proton dynamics in coal, *J. Non-Crystall. Solids* 188 (1-2) (1995) 161-168. [https://doi.org/10.1016/0022-3093\(95\)00101-8](https://doi.org/10.1016/0022-3093(95)00101-8)
160. C. Cachet, A. Belushkin, I. Natkaniec, A. Lecerf, F. Fillaux, L.T. Yu, Characterization with inelastic neutron-scattering of various Protonic species in manganese oxides, *Physica B* 213 (1995) 827-829. [https://doi.org/10.1016/0921-4526\(95\)00293-l](https://doi.org/10.1016/0921-4526(95)00293-l)
161. R. BaddourHadjean, F. Fillaux, J. Tomkinson, Proton Dynamics in eta-Ni(OH)(2) and eta-NiOOH, *Physica B* 213 (1995) 637-639. [https://doi.org/10.1016/0921-4526\(95\)00235-2](https://doi.org/10.1016/0921-4526(95)00235-2)
162. P. Alers, G. Prescher, F. Fillaux, Inelastic neutron scattering study of proton dynamics in caron lacks, *Carbon* 34 (7) (1996) 903-908. [https://doi.org/10.1016/0008-6223\(96\)00042-5](https://doi.org/10.1016/0008-6223(96)00042-5)
163. F. Fillaux, S.M. Bennington, L.T.L. Yu, Inelastic neutron-scattering study of free proton dynamics in gamma-MnO₂, *Chem. Phys.* 209 (1) (1996) 111-125. [https://doi.org/10.1016/0301-0104\(96\)00140-1](https://doi.org/10.1016/0301-0104(96)00140-1)
164. F. Fillaux, New proton dynamics in solids revealed by vibrational spectroscopy with neutrons, *J. Mol. Struct.* 511 (1999) 35-57. [https://doi.org/10.1016/S0022-2860\(99\)00140-4](https://doi.org/10.1016/S0022-2860(99)00140-4)
165. F. Fillaux, New proton dynamics in solids revealed y virational spectroscopy with neutrons, *Solid State Ionics* 125 (1-4) (1999) 69-79. [https://doi.org/10.1016/S0167-2738\(99\)00160-5](https://doi.org/10.1016/S0167-2738(99)00160-5)
166. F. Fillaux, C. Cachet, S.F. Parker, J. Tomkinson, A. Quivy, L.T. Yu, Inelastic neutron scattering studies of the proton dynamics in bi-doped manganese oxides, *J. Electrochem. Soc.* 147 (11) (2000) 4184-4188.
167. F. Fillaux, S. Menu, J. Conard, H. Fuzellier, S.W. Parker, A.C. Hanon, J. Tomkinson, Inelastic neutron scattering study of the proton dynamics in HNO₃ graphite intercalation compounds, *Chem. Phys.* 242 (2) 1999, 273-281. [https://doi.org/10.1016/S0301-0104\(99\)00022-1](https://doi.org/10.1016/S0301-0104(99)00022-1)
168. S. Deng, Y. Zhang, Location and lattice dynamics of a proton in the perovskite structure, *phys. Status solidii* 253 (9) (2016) 1688-1696. <https://doi.org/10.1002/pssb.201600063>
169. A. Braun, Q. Chen, Experimental neutron scattering evidence for proton polaron in hydrated metal oxide proton conductors, *Nature Comm.* 8 (2017) 15830 [doi:10.1038/ncomms15830](https://doi.org/10.1038/ncomms15830).
170. P. Colomban, Latest developments in proton conductors, *Ann. Chim. Sci. Mat.* 24 (1999) 1-18. [https://doi.org/10.1016/S0151-9107\(99\)80030-0](https://doi.org/10.1016/S0151-9107(99)80030-0)
171. K.D. Kreuer, On the development of proton conducting materials for technological applications, *Solid State Ionics* 97 (1997) 1-15. [https://doi.org/10.1016/S0167-2738\(97\)00082-9](https://doi.org/10.1016/S0167-2738(97)00082-9)

172. S. Shin, H.H. Huang, M. Ishigame, H. Iwahara, Protonic conduction in the single crystals of SrZrO₃ and SrCeO₃ doped with Y₂O₃, *Solid State Ionics* 40/41 (1990) 910-913. [https://doi.org/10.1016/0167-2738\(90\)90151-G](https://doi.org/10.1016/0167-2738(90)90151-G)
173. H. Yugami, Y. Shiayama, T. Hattori, M. Ishigame, Proton diffusivity in SrZrO₃: Sc³⁺ single crystals studied by infrared absorption spectroscopy, *Solid State Ionics* 79 (1995) 171-176. [https://doi.org/10.1016/0167-2738\(95\)00057-D](https://doi.org/10.1016/0167-2738(95)00057-D)
174. H. Yugami, Y. Shiayama, S. Matsuo, M. Ishigame, S. Shin, Proton sites and defect-interactions in SrZrO₃ single crystals studied by infrared absorption spectroscopy, *Solid State Ionics* 85 (1996) 319-322. [https://doi.org/10.1016/0167-2738\(96\)00076-8](https://doi.org/10.1016/0167-2738(96)00076-8)
175. T. Scheran, Y.M. Baikov, E.K. Shalkova, H⁺/D⁺ isotope effect in Y-doped BaCeO₃ crystals, *Solid State Ionics* 66 (1993) 159-164. [https://doi.org/10.1016/0167-2738\(93\)90039-6](https://doi.org/10.1016/0167-2738(93)90039-6)
176. A. Pons, E. Béchade, J. Jouin, M. Colas, P.-M. Geffroy, O. Masson, P. Thomas, I. Kagomiya, T. Asaka, K. Fukuda, A. Slodczyk, P. Colomban, Structural modifications of lanthanum silicate oxyapatite exposed to high water pressure, *J. Eur. Ceram. Soc.* 37 (2017) 2149-2158. : [10.1016/j.jeurceramsoc.2016.12.034](https://doi.org/10.1016/j.jeurceramsoc.2016.12.034)
177. A. Slodczyk, P. Colomban, N. Malikova, O. Zaafrani, S. Longeville, J.M. Zanotti, O. Lacroix, B. Sala, bulk protons in anhydrous perovskites-neutron scattering studies, *Solid State Ionics* 252 (2013) 7-11. <https://doi.org/10.1016/j.ssi.2013.06.012>
178. A. Slodczyk, M.H. Limage, P. Colomban, O. Zaafrani, F. Grasset, J. Loricourt, B. Sala, Substitution and proton doping effect on SrZrO₃ behaviour: high-pressure Raman study, *J. Raman Spectrosc.* 2011 <https://doi.org/10.1002/jrs.2968>